# A Parametric Model for Reducing the Manufacturing Cost of the Traveling Wave Tube

by

Mark L. Homer

Submitted to the Department of Mechanical Engineering on May 12, 1993, in partial fulfillment of the requirements for the degrees of Bachelor and Master of Science in Mechanical Engineering at the MASSACHUSETTS INSTITUTE OF TECHNOLOGY May 1995



Author.....

Department of Mechanical Engineering

May 9, 1995

Certified by.....

Daniel E. Whitney

Lecturer, Department of Mechanical Engineering

Thesis Supervisor

Certified by.....

Ed Bernardon

Technical Staff, C. S. Draper Laboratory

Thesis Supervisor

Accepted by.....

Ain A. Sonin

Chairman, Departmental Committee of Graduate Students

# A Parametric Model for Reducing the Manufacturing Cost of the Traveling Wave Tube

by

Mark L. Homer

Submitted to the Department of Mechanical Engineering on May 12, 1993, in partial fulfillment of the requirements for the degrees of Bachelor and Master of Science in Mechanical Engineering

## Abstract

Placing tight specifications on a product's performance tends to raise the cost to produce it. The Naval Research Laboratory wants to help systems designers that use the Traveling Wave Tube (TWT) to understand this tradeoff. A computer tool was developed which allows the user to predict the TWT's unit cost based upon its specifications. Tradeoff curves can thus be constructed to help buyers of the TWT to issue specifications that strike the right balance between price and performance. To find the cost associated with a given set of specifications, the set of processing options that creates a tube whose performance meets all requirements at the lowest cost must be found. Essentially, an optimization problem must be solved. The user can either manually or automatically (through an algorithm called simulated annealing) search through processing options to find the lowest cost solution. A set of mathematical functions connect manufacturing choices to cost and performance. Organization, acquisition, and description of these links are detailed. Interviews with experts and published research were primarily used to construct the relations. Much effort was spent in trying to simplify the modeling effort. To demonstrate the computer tool, test cases are provided. In both manual and automatic search, the tool finds low cost solutions. Throughout the discussion, the tool's capabilities and limitations are identified.

| | |
|---|---|
| Thesis Supervisor: | Daniel E. Whitney |
| Title: | Lecturer, Department of Mechanical Engineering |
| Thesis Supervisor: | Ed Bernardon |
| Title: | Technical Staff, C. S. Draper Laboratory |

## Acknowledgements

To Ed Bernardon, Dr. Daniel Whitney, "the engineer," Todd Hamilton, all those in the ADT group at C.S. Draper Laboratory, and my family (especially Amy, my partner in life) I say thank you.

# Contents

# Chapter One

# Introduction

As a product's specifications become more stringent, the cost to make the product tends to rise. The demand for better functionality constrains the designer from choosing lower cost options. In essence, a tradeoff exists between high performance and low cost. The specifications for a product must be chosen carefully to insure that a correct balance has been struck.

The Naval Research Laboratory (NRL) has hired C.S. Draper Laboratory to help the Microwave Power Module (MPM) industry better understand this tradeoff. As part of my work under the Engineering Internship and Draper Fellows Programs, I have had the fortune to participate in this project. The MPM, a recently conceived device, amplifies microwave signals in the 2 to 40 GHz range. The NRL sees the potential for the use of such a device in a broad variety of applications, including radar and electronic countermeasure applications found in the military. By using one basic product design for a variety of applications, the government hopes to reap a substantial cost savings. Broad applicability means high production volume which in turn translates into low manufacturing cost. The United States military, by far the biggest customer of systems that need microwave amplifiers, hopes to benefit from this cost reduction.

Figure 1-1 shows two applications and the performance they require. Instantly, one notices the disparity between their the requirements. MPMs for radar applications require high power but do not function over a broad frequency bandwidth. MPMs for electronic countermeasure applications lie in a completely opposite situation. Even within a particular application area, performance requirements can vary. For example, phased radar arrays have stringent size requirements. Worse, the exact size limits can vary from one phased radar system design to another. Therefore, each production order is expected to contain its own set of tailored specifications.

| PARAMETER | ELECTRONIC WARFARE | RADAR |
|---|---|---|
| frequency | 6-18 GHz | 7-11 GHz |
| power | 50-100 W | 100 W |
| duty cycle | continuous | 50% |
| gain | >50 dB | > 50 dB |
| efficiency | >33 % | > 40 % |
| noise power density | < -10 dB | < -157 dBc/Hz |
| size | 5/16" x 4" x 6" | 1" x 2" x 6" |
| harmonics | > -10 dBc | > -60 dBc |

Figure 1-1: Two Applications for the MPM and Their Specifications

By design, the basic concept of the MPM is flexible enough to handle these disparate demands. However, detailed aspects of the product's design will still need to be changed with each production order. The designers of the MPM must choose the correct design for each order that minimizes the cost to produce it while meeting all performance specifications. The MPM consists of three major sub-components: the electronics power conditioner (EPC), the solid state amplifier (SSA), and the traveling-wave tube (TWT). Both the SSA and the TWT are microwave amplifiers. The EPC conditions the power sent to both the SSA and the TWT. The input signal is first sent to the SSA and then the TWT In this sense, the MPM is a two stage amplifier. Figure 1-2 is a conceptual diagram of the MPM and the relationship among its sub-components. Usually, the company that integrates the sub-components into the MPM buys the sub-components from suppliers. Inevitably, changes in MPM specifications alter those at the sub-component level. The sub-components' manufacturers build their products to the specifications handed down from the MPM companies. Many options exist for allocating these sub-component specifications. The systems integrator has the freedom to divide the total gain of the MPM between the TWT and SSA. The performance allocation that minimizes the combined cost of the sub-components needs to be found. Therefore, systems integrators require a firm understanding of how the sub-components' performance specifications affect their respective costs.

Currently this understanding is achieved by asking the sub-component designers. The MPM integrator compiles a set of specifications for each of the three sub-components. All sub-component suppliers are asked to make cost estimations based on this set. The system engineers repeat this process over several different sets. Figure 1-3 depicts a flow chart of this process. The whole effort can take months as the individual cost estimates require approximately a week to complete. Both the systems integrators and NRL recognize that the process is too time consuming. Project schedules prevent the identification of good allocation strategies. My group at C.S. Draper Laboratory believes this process could be improved if the systems integrators could understand the tradeoff between cost and performance within the sub-components more quickly.

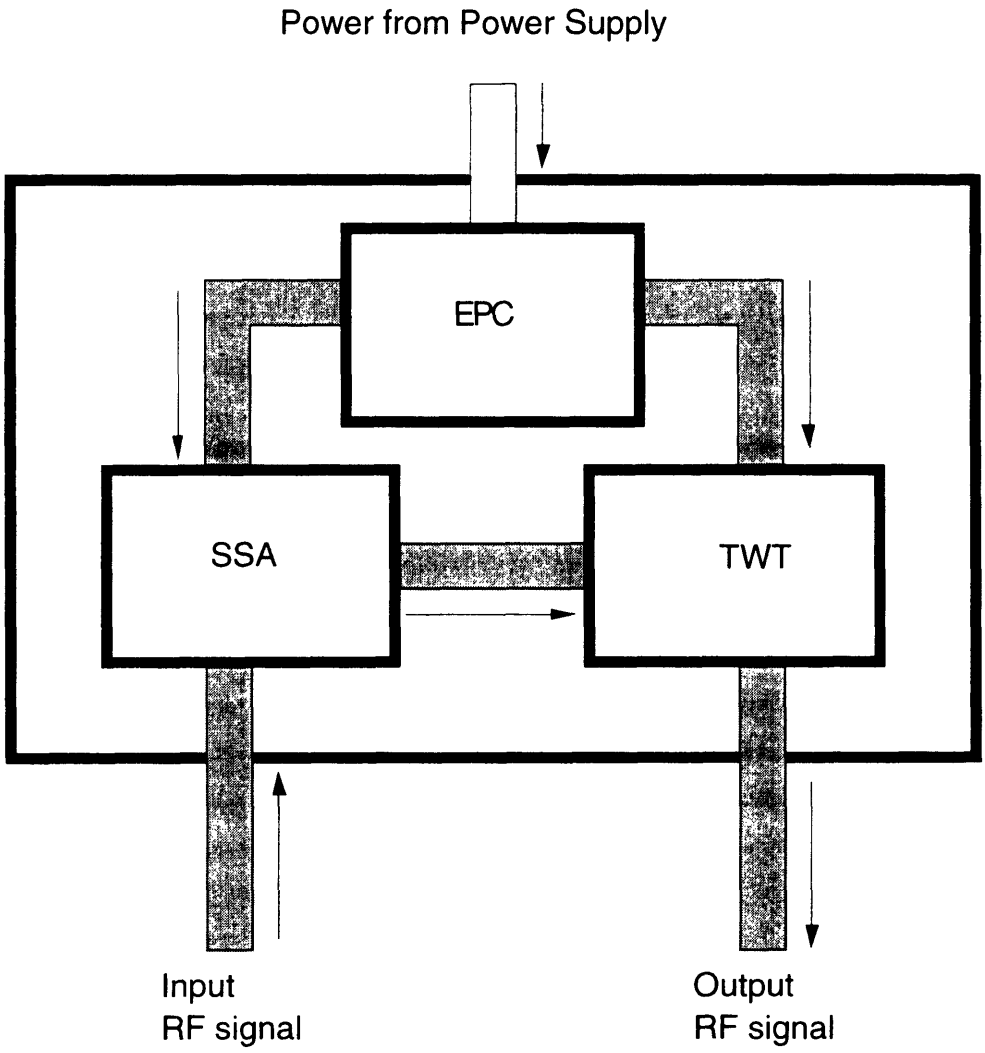


Figure 1-2: Relationship Between MPM Sub-Components

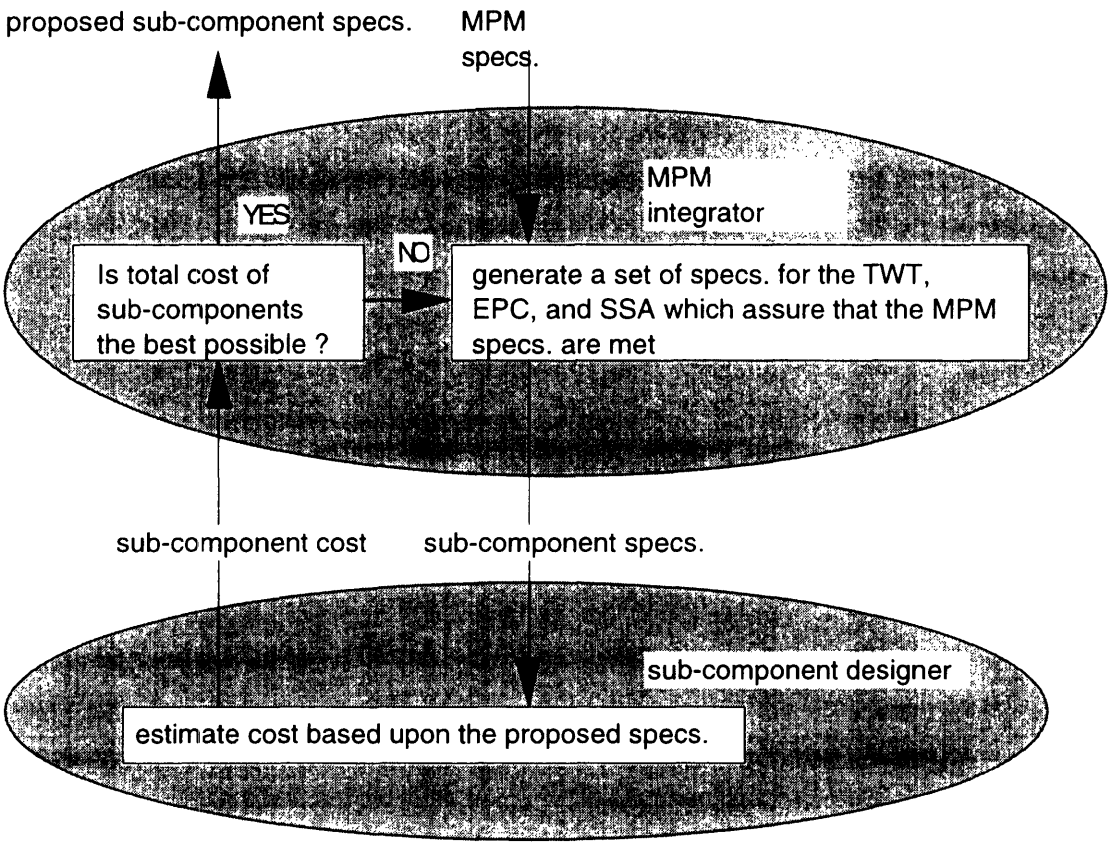


Figure 1-3: Flow Chart of Sub-Component Specification Process

My group is creating a computer tool that can estimate the sub-components' costs based on their respective performance specifications. The tool will give systems integrators an instant understanding of the tradeoff between cost and performance. The optimum allocation of specifications can be approached faster, leading to lower cost MPM designs. The computer tool will use expert knowledge. Design and manufacturing engineers have been asked to fill out questionnaires. For each sub-component, cost estimations are performed for several specification combinations. The computer program automatically fits a multi-dimensional curve to this data. Users can thereby obtain manufacturing cost at any point between the data points collected.

Follow on contracts exist to capture the relationship between performance and cost at a deeper level. This thesis proposes an approach and develops a computer tool prototype to evaluate the methodology's effectiveness. The study was performed on one particular manufacturer's TWT. The connection between cost and performance is made by specifically taking into account the product's design and factory setup. The linking is done through a series of mathematical relationships. Demanding performance specifications constrain a product's design from low cost options. The processing plans determine the physical embodiment of the TWT's design. A computer model is constructed which allows the user to set the product's specifications and choose from a fixed set of possible manufacturing strategies. For each manufacturing configuration, the computer tool can calculate the unit cost and determine the resulting design's ability to meet the desired performance measures. Users can then search through the various processing options (such as the decision to electroplate specific components) until the lowest cost design is found that meets all the specifications. The search process can either be done manually or automatically through a search algorithm called simulated annealing. The whole process is essentially transformed into an optimization problem with cost as the value to minimize, the performance specifications as the constraints to be satisfied, and processing options as the set of solutions from which to choose. By casting the specification to cost problem into the optimization framework, a more detailed estimation of cost can be produced.

In Chapter 2, the current estimation process used to translate specifications to cost is detailed. Efforts by [Ramaswamy, 1993] and [Milner, 1991] are then discussed to show how the estimation process can be modeled

as the solving of an optimization process. The chapter ends by depicting the cost tool's internal structure using this optimization framework. Chapter 3 focuses on the link between performance and design. A general description of the TWT is provided. Steps to reduce the modeling effort and the actual equations used during this linking follow. Chapter 4 examines the connection between processing options, design, and cost. The manufacturing process at the plant studied is highlighted and used in combination with a brief discussion of various cost estimation methodologies (including those used at the plant) to provide background for the cost estimation method used in this thesis. The various processing techniques captured by the model and their influences on cost and design are then detailed. The interface is explained in Chapter 5. Both manual and automatic search routines are described and test cases are given to show their effectiveness. Chapter 6 summarizes the conclusions drawn from the thesis project, including an evaluation the tool's utility.

# Chapter Two

# General Structure

## 2.1 Overview

This section details the current methodology TWT designers utilize to calculate cost from performance. This process is shown to be equivalent to solving an optimization problem. A general representation of this problem is then shown, revealing the general structure of the computer tool.

## 2.2 The Cost Estimation Process

The first step in defining functional links between specification and cost was to understand the current estimating process. Six companies manufacture the TWT: Teledyne, Litton, Varian Associates, Northrop-Grumman, ITT Defense and Electronics, and Hughes. TWT product and manufacturing engineers were interviewed at each of the companies. The discussions revealed the iterative nature of the cost estimation process. During each iteration, a design is generated which is thought to satisfy all performance requirements at a low cost. Designers subsequently check the design's performance and calculate its cost. The number of iterations is primarily contrained by time limitations. The lowest cost among those designs which meet all specifications is chosen as the cost associated with the given performance specifications. The nature of the proposed design determines the exact method for testing its performance and estimating its cost. Designs roughly fall into three catagories: past, innovative, and revolutionary.

Past designs have been produced for customers in the past. Companies have past data on their performance and manufacturing cost. Estimation is simply a matter of finding this information.

Innovative designs only vary slightly from those of the past. Although these designs have never made it to full scale production, empirical evidence supports their feasibility. Proof comes from academic research or the company's own R&D studies. Computer simulations are used heavily to check the product's performance. Occasionally, prototypes are even built and tested. The engineers base manufacturing cost upon the resources needed to

manufacture the design. Since the product's design does not differ greatly from those made before, most manufacturing activities do not change from those of the past. Cost for these activities are based on past data. Newer activities require deeper thought. The estimator guesses what the lowest cost process plan will be and projects the amount of labor, material, and equipment resources. Many times, values are derived from extrapolation of current processes. For example, a 12 part assembly is estimated to take 30 minutes of labor, if a similiar design with 6 pieces takes 15 minutes. Such estimations are only gross approximations. Errors typcially can grow to as high as 100% of the actual value. The inaccuracy is largely due to uncertainty in the details of the envisioned process plan.

Revolutionary designs experiment with new, untested principles. Such designs have no guarantee of working. Even if workable, they might require months of development time. Since the detailed design of the product is not known, the manufacturing processes needed to create it can not be envisioned. For this reason, cost estimation is not done at any detailed level. At best, guesses based on past experience are provided when dealing with untested technology.

Since the MPM was concieved to save the government money, the MPM integrators do not plan to issue specifications that push the design into untested and therefore costly grounds. On the flip side, most MPM integrators do not expect the design to be completely based on those of the past. The MPM needs to appeal to a large and varied contingent of customers. Clearly, the proposed TWT designs will iterative in nature.

## 2.3 The Optimization Framework

[Ramaswamy, 1993] descibes a similiar process at a car company. Designers use a commercial CAD system to find designs that meet a given set of specifications. Figure 2-1 shows a piece of the model. Causality moves from left to right. For instance, the tire radius influences the transmission ratio change which in turn influences the fuel efficiency. Let the values inputted into the model, like tire radius and brake type, be called the design parameters. Similiarly, let its outputs (fuel efficiency and braking deceleration) be labeled performance parameters.

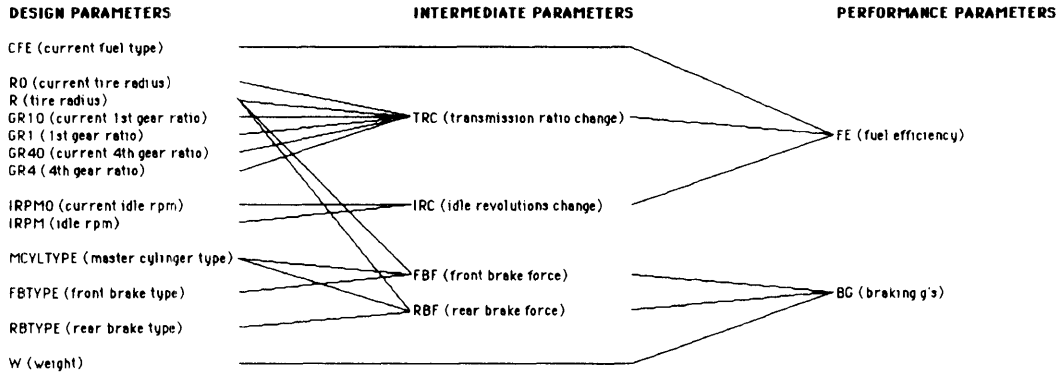


Figure 2-1: A Section of Ramaswamy's Car Model

The performance parameters are linked to the design variables through a set of mathematical equations and intermediate variables. Marketing gives the designers a set of specifications that they are required to meet. The designers change the design parameters until the calculated performance parameters meet the specifications. The designers continue to propose new designs and evaluate them until a feasible design is found. Experienced designers can take a day or two to find an acceptable design. Ramaswamy notes that multiple solutions are not found due to time constraints. This process of proposing a design and then checking its performance is similiar to the one in the TWT industry. Ramaswamy then proceeds to represent the process as the solving of an optimization problem. The diagram in Figure 2-1 can be converted into a more quantitative description through the use of mathematical functions. With such a set of functions it is possible to mathematically state the problem faced by the car designers. Suppose the specifications for the car were a fuel efficiency and deacceleration of no less that 15% and 0.25 g's respectively. The problem can be mathematically interpretted as:

*Find*

$CFE, RO, R, GR10, GR1, GR40, GR4, IRPM0,$

$IRPM, MCYLTYPE, FBTYPE, RBTYPE,$ *and* $W$

*such that*

$$
\begin{aligned}
&TRC(\, R0, R, GR10, GR1, GR40, GR4\,) = TRC \\
&IRC(\, IRPM0, IRPM\,) = \boldsymbol{IRC} \\
&FBF(\, R, MCYLTYPE, FBTYPE\,) = \boldsymbol{IRC} \\
&RBF(\, R, MCYLTYPE, RBTYPE\,) = \boldsymbol{IRC} \\
&FE(\, CFE, TRC, IRC\,) \in \boldsymbol{FE} \\
&BG(\, FBF, RBF, W\,) \in \boldsymbol{BG}
\end{aligned}
\qquad (2\text{-}1)
$$

where the notation $F(\, A, B\,)$ denotes the function that maps the parameters A and B to F, $\boldsymbol{F}$ decribes the set of allowable values for F, and all other variables are as shown in Figure 2-1.

In the problem faced the by TWT designers, cost must be minimized as well as performance measures satisfied. [Milner, 1991] deals with the cost minimization aspect. Milner concentrates on finding the assembly sequence for a given product design that minimized the cost to make it. As each assembly sequence is considered, the minimum cost assembly line design is

determined. This creates a whole new sub-problem called the equipment selection and task assignment problem (ESTA). The ESTA problem highlights how aspects of a product's design are connected to cost through manufacturing system and process design choices. Decisions about the product's process plan determine both its cost and performance.

Combining Ramaswamy's and Milner's views allow the determination of cost from performance specifications to be recast as the solving of an optimization problem. The problem can be mathematically generalized using set notation:

$$\min\left[\, Cost(M) \,\right]$$

*such that*

$$D = D(M) \qquad (2\text{-}2)$$

$$P(D) \in \boldsymbol{P}$$

$$M \in \boldsymbol{M}$$

where M, D, P describe a proposed product's process plan, design, and performance, Cost() is the function that maps M to unit cost, D() maps to M to D, P() maps D to P, and **M** and **P** are the sets which must respectively contain M and P.

Designers tend to think of a product's design determining its function, not a product's function determining its design. The same holds true for cost. The process plan determines cost and the product's key physical attributes. Science is built around this idea of such causality. Once the process plan is defined for a given product, there exists only one value for cost, the set of design features, and performance values. The same does not hold true for going in the reverse direction. In some sense design and optimization address the issue of going backwards. We know what output we want; we need to know what input values to put in. Unforetunately, there usually exists no easy way of inverting the problem statement. Thus, one is confined to choosing designs, or (in optimization terminology) points in the input space, and calculating the values in an iterative manner until the correct value is found.

The structure of the computer program constructed is based upon equation set 2-2. First, the user defines the allowable region of performance values ( **P** ). Process plans ( M ) can then be chosen from a set of possible choices ( **M** ) and evaluated. The tool contains sets of mathematical functions

which operate as D(), Cost(), and P() in equation set 2-2. Manual iteration or the use of the simulated annealing algorithm can be used to search through possible choices for M. The goal during the searches is to find the M that minimizes the reported cost without violating any of the stated specifications.

# Chapter Three

# Linking Performance to Design

## 3.1 Overview

This chapter describes the mapping of the TWT's design to its performance. A high level description of the TWT and the key phenomena that occur within it are provided. Methods used to reduce the modeling effort follow. A description of the model's major parts are detailed. The final section is reflective in nature, measuring the success of the modeling strategies employed.

## 3.2 Brief Description of TWT Physics

The following sub-sections provide a brief description of the TWT's major components and functionality. Three books provide further detail. [Pierce, 1950] established the terminology and basic approach for analyzing the TWT. Much of the description below was adopted from [Gilmour, 1994]. The book provides a comprehensive description of the TWT and basic methods for analyzing its performance. [Rowe, 1965] delves deeper into the physics of the beam-wave interaction. However, deep knowledge of electrodynamics is required to fully grasp the derived results.

### 3.2.1 General Description

Figure 3-1 is a conceptual diagram detailing the major parts of the TWT. The microwave signal is amplified by its interaction with an electron beam generated by the gun. A set of periodic magnets prevents the beam from spreading as it travels down the central axis of the TWT. The microwave propagates down the tube at approximately 1/10 the speed of light, slowed by the helix structure. The beam, which travels at a slightly faster speed, transfers energy to the RF signal. Thus, the microwave signal is amplified. The remaining energy in the beam not transferred to the microwave signal is caught by the collector.

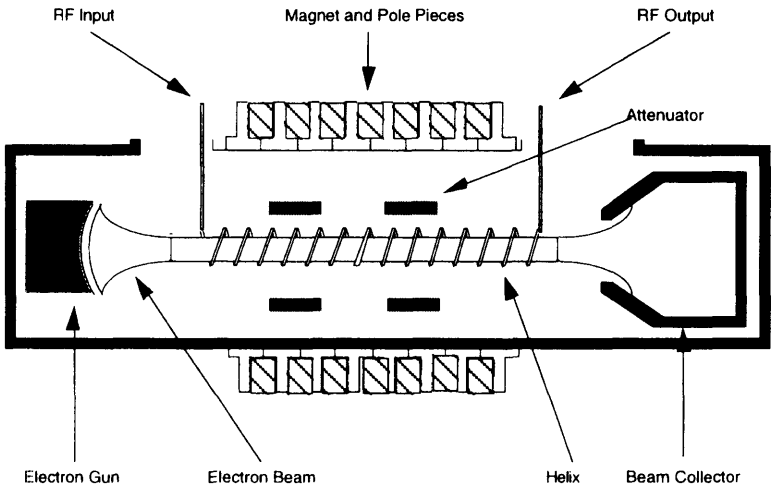


Figure 3-1: Conceptual Diagram of the TWT (Adapted from [Gilmour, 1994])

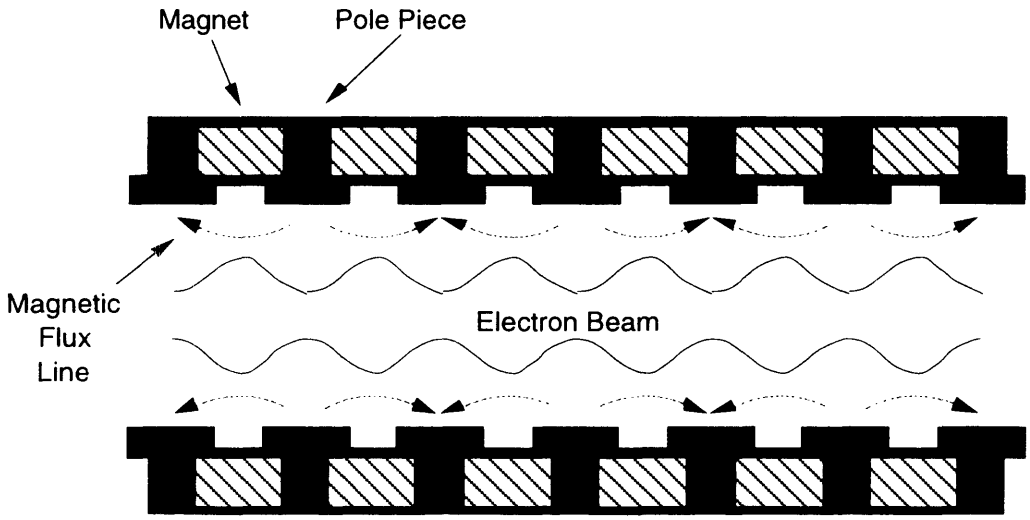


Figure 3-2: Magnet Arrangement and Beam Shape
(Adapted from [Gilmour, 1994])

### 3.2.2 Beam Generation and Focus

Guns generally consist of a cathode and a set of focusing electrodes. The cathode generates the electrons that are focused and accelerated to form the intense electron beam. Cathodes are constructed from a mixture of metals such as tungsten and barium. A heater typically maintains the mixture at 1100 °C to insure high emission rates. As the electrons emerge from the cathode's surface, a negative voltage potential accelerates them toward the helix. A set of focusing electrodes shape the potential field, tightly bunching the beam. The base TWT design under study generates beams with a potential of 4475 kV, a current of 0.15 A, and a diameter of 0.76 mm.

### 3.2.3 Beam Maintenance

As the beam travels down the central axis, the electrons in the beam repel each other. To prevent the beam from expanding in diameter and striking the helix, a magnetic field is used to counteract this force. The size and weight of a TWT functioning in an MPM must be minimized. Therefore, the magnetic field is created by a series of permanent magnets as opposed to a solenoid. The periodicity of the magnetic field forces the beam to take on a "scalloped" appearance as shown in Figure 3-2. The entire region within the outer metallic shell holds a vacuum of from 1*10 -7 to 1*10 -9 torr depending upon the particular design. This prevents the beam from colliding with particles in its path.

### 3.2.4 Electron-Wave Interaction

The beam interacts with the microwave signal along the helix structure. The RF signal propagating down the tube travels along the helical path close the speed of light. As a result, the axial speed of the wave's propagation is much slower. The beam's speed is controlled by the voltage applied to it. The TWT's voltage and pitch are set such that the electron beam travels slightly faster than the RF wave. The oscillating electric field patterns of the wave during its propagation are shown in Figure 3-3. These fields attract the electrons in the beam to regions marked "A" and away from regions marked "B." An electron bunch starts to form in region "A." Electrons on the helix moving with the RF wave will be repelled from the "A" regions by these bunches. This strengthens the field between the helix

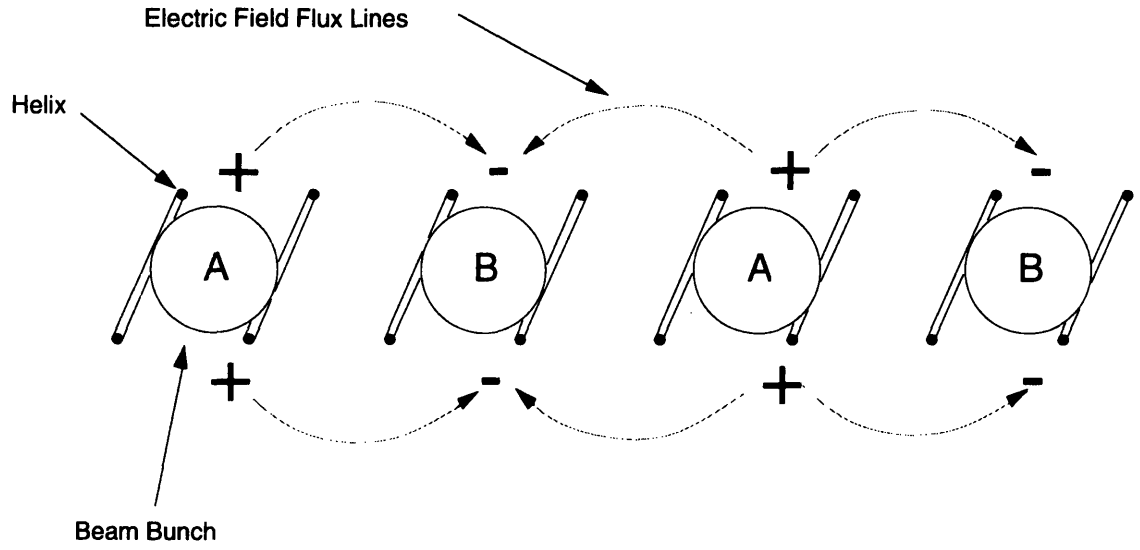


Figure 3-3: Electrical Field Patterns and Beam Bunching During the Beam-Wave Interaction (Adapted from [Gilmour, 1994])

coils which in turn creates tighter beam bunching. The whole process can be thought to continue in this circular manner resulting in an exponential growth in the microwave's field strength. This energy transfer causes the electron beam to decelerate. Eventually, the beam falls out of synchronism with the wave form and the process saturates.

Unfortunately, the helix is a dispersive circuit. The velocity of the wave is a function of frequency. The wave's velocity needs to be close to that of the beam's to insure signal gain. Therefore, gain only occurs over a certain range of frequencies in the TWT. Frequency's effect can be lessened by "loading" the tube. Figure 3-4 shows a cross section of a loaded tube. The support rods' material and geometry as well as those of the metallic vanes' act to reduce the dispersion. Loading reduces the efficiency of the beam-wave interaction but allows the tube to function over a wider bandwidth.

### 3.2.5 Beam Collection

After the beam leaves the helix, it enters the collector. Collectors have a series of depressed voltages applied to them. The number ranges from one to five. Figure 3-5 shows the inside of a collector with four depressed voltage levels or stages. The voltage depressions decelerate the electron beam, reducing power lost to heat. The more levels, the more efficient the collector is in recouping the leftover energy within the beam. Collector design has a direct impact on the TWT's efficiency.

## 3.3 Problem Simplification

The above simplified description of the TWT hints at the complexity of its design. The designer must consider thousands of design details to assure proper functionality. He must track a vast number of interconnections between the design and performance. I employed strategies in an attempt to simplify the task of mathematically modeling these interconnections. A designer at one of the TWT manufacturers had an intuitive grasp of the important design parameters in TWT design. For proprietary purposes, the designer's and company's names will be replaced with the terms "the engineer" and "the manufacturer." Initial discussions with the engineer suggested that only a few key performance parameters drove the product's cost. In response, I asked specific questions to the engineer during phone conversations and in a questionnaire which identified the key performance

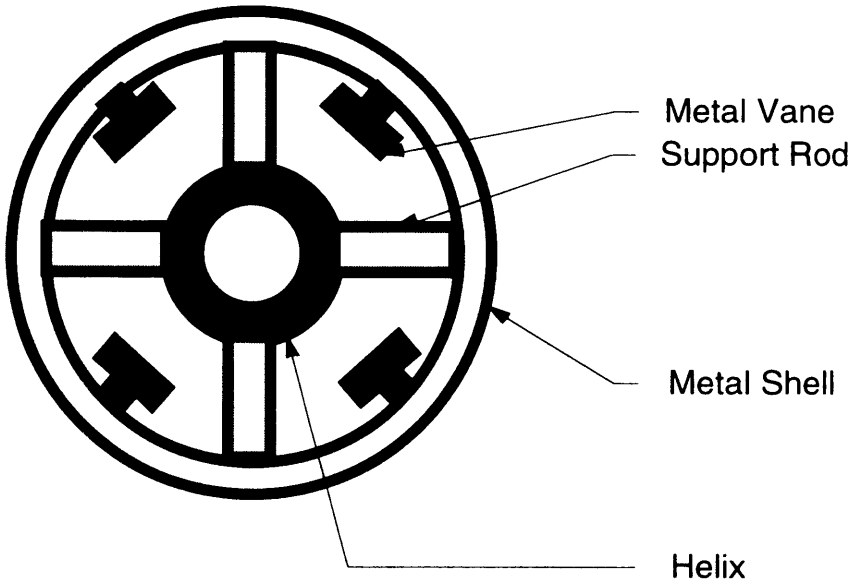


Figure 3-4: Cross Section of a Loaded TWT

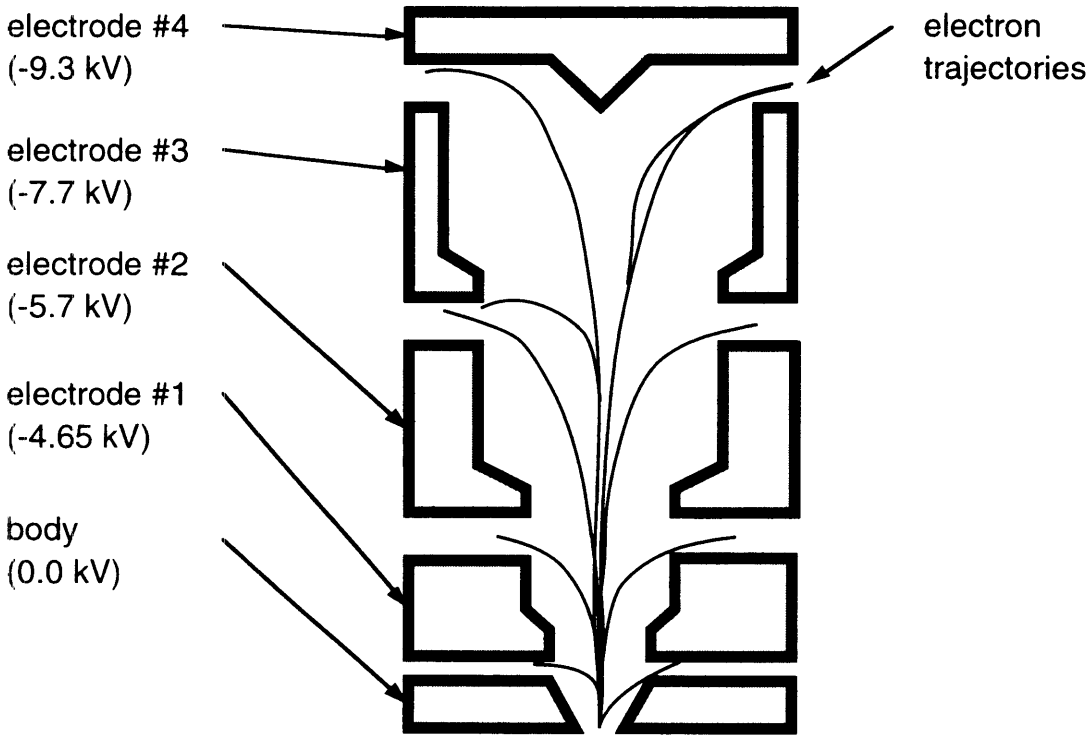


Figure 3-5: Cutaway of a Four Stage Collector
(Adapted from [Gilmour, 1994])

parameters, design parameters, and the interactions between them. The answers successfully reduced my modeling effort.

### 3.3.1 Identifying the Key Performance Parameters

The first step in the linking of design to performance was to determine the specifications that had the greatest impact on cost. The investigation focused specifically on TWT's designed for integration into MPM's. Within the MPM program, each specification is expected to vary within a specified range. It is important to identify those specifications that most influence cost over these ranges. The engineer was asked to draw from his experience in working with a particular design whose performance range covered those expected to be requested by the MPM integrators. The important specifications along with there expected range are shown in Figure 3-6.

### 3.3.2 Identifying the Key Design Parameters

Once the key specifications were identified, the next challenge was to reduce the number of parameters needed to describe the TWT's design. Initial discussions with the engineer revealed that many of the design variables would not change over the range of performance demanded by the MPM. Fixing unchanging design variables reduced the modeling effort significantly. The gun design is a perfect example. Its design will not change in the TWT's used in MPM. A screw is used to slightly change the gun's performance for each specific tube design. A design parameter called perveance captures this adjustability. No other details or physics of the gun need to be modeled to understand its influence on performance.

Figure 3-7 summarizes the key design areas and their influence on the important performance measures. The matrix also includes the range for each performance parameter over which this information is relevant. An "x" in row i and column j denotes that the design parameter in row i impacts the performance parameter in column j. A "<," ">," or "</>" denotes whether the specification on that performance measure is a lower, upper, or combination upper and lower limit.

| Specification | Least Stringent Value Requested by Systems Designers | Most Stringent Value Requested by Systems Designers |
|---|---|---|
| Max. Output Power | 10 Watts | 150 Watts |
| Efficiency | 7% | 30% |
| Small Signal Gain | 25 ± 3 dB | 75 dB ± 0.5 dB |
| Beam Voltage | 1.5 KV | 4.5 KV |
| Beam Current | 0.050 A ± 10% | 0.175 A ± 1% |
| Harmonic Power | 0 dBc | (- 15) dBc |
| Length | 10.0 inches | 4.0 inches |
| Diameter | 1.25 inches | 0.75 inches |
| Phase Shift | ±30° | ±10° |
| Noise Power | 10 dBm/MHz | (-16) dBm/MHz |

Figure 3-6: Cost Influencing Specifications and Their Range of Values

| DESIGN CHOICES | SPECIFICATIONS | | | | | | | | |
|---|---|---|---|---|---|---|---|---|---|
| | Output Power | Efficiency | Small Signal Gain | Beam Current | Harmonic Power | Length | Diameter | Phase Shift Tolerance | Noise Power |
| | > | > | </> | </> | < | < | < | < | < |
| | 10 to 150 Watts | 7 to 50% | 25 to 75 dB ± 3 to 1 dB | 0.050 to 0.175 A ± 10 to 1% | 0 to -15 dB | 10 to 4 in. | 1.25 to 0.75 in. | ±30° to ±10° | 10 to -16 dB/MHz |
| conductivity of helix | X | X | X | | X | | | X | X |
| helix radius | X | X | X | | X | | | X | X |
| helix pitch | X | X | X | | X | | | X | X |
| helix axial length | X | X | X | | X | X | | X | X |
| thermal resistivity of bundle and shell | | | | | X | | | X | X |
| material choice for support rods | X | X | X | | X | | | X | X |
| number of rods | X | X | X | | X | | | X | X |
| shell to helix radius | X | X | X | | X | X | | X | X |
| vane height | X | X | X | | X | X | | X | X |
| gun perveance | X | X | X | X | X | X | | X | X |
| collector efficiency | X | X | | | | X | | | |

Figure 3-7: Design to Performance Matrix

### 3.3.3 Modeling the Individual Connections

Examination of the matrix reveals the design's complexity. Most of the design variables influence most of the performance parameters. For example, there are 13 design parameters that influence small signal gain. The engineer could describe with curves or a few simple rules of thumb the impact of two or three design parameters on a performance parameter if the other design parameters were fixed to known values. He could not describe changes beyond three. In fact, computer simulations were routinely used to check the performance of TWT designs at the manufacturer. These simulations were quite complex relying on years of research. The simulations required the computer to solve a set of non-linear partial differential equations or to utilize the techniques of finite element analysis. Unfortunately, the simulation models could not be incorporated into the modeling effort in this thesis. Current computational tools do not incorporate the influence of all the important design parameters listed in Figure 3-7. In addition, their runs times ranged from 10 to 20 minutes on small sized workstations. Such long run times would prevent the evaluation of a large number of process design options. The computational expense would severely limit the effectiveness of the search process.

Unable to use expert knowledge or existing simulations, I followed the only option, namely was to turn to published research. Experts from the manufacturer and other TWT manufacturers were able to aid in the location of this research. Finding computationally inexpensive models that covered all the essential design parameters required extensive legwork in libraries. Fortunately, prior work had been done to divide the physics into distinct sectors. The calculation of small signal gain serves as an example. One model was found that predicted the propagation characteristics of the helix. The propagation characteristics were then used in another set of calculations to predict the small signal gain. Intermediate variables such as the helix's propagation characteristics allowed the modeling to be broken up into manageable pieces.

## 3.4 Model Description

Figure 3-8 shows the key pieces of the model I constructed and the variables that connect them. For example, the beam current module calculates beam DC current (i0) from the perveance of the gun (gun_perv) and the operating cathode voltage (V0). This fact is denoted by two "x" marks in the gun_perv and V0 row under the i0 column. Within the beam DC current module is an analytical equation which performs the computation. Only 7 out of the 10 performance parameters listed in Figure 3-7 were modeled. No closed form solutions were found which even roughly predicted phase shifts and harmonic power within the tube. The task of incorporating these phenomena was judged too difficult under the time constraints of this thesis. Time limitations also prevented the incorporation of the noise power. Methods must be found to capture the influence of phase shift, harmonic power, and noise. Although the model stands incomplete without the inclusion of these specifications, the basic concept behind it still can be evaluated to judge its worth.

### 3.4.1 Adjustable Design Parameters

The following is a list of the design parameters the user or automatic search routine is allowed to change.

**helix_radius** - average of the helix's inner and outer diameter (See Figure 3-9)

**phratio** - ratio of the helix's pitch to its average radius

The pitch of the helix is defined as the distance between adjacent turns of the helix (See Figure 3-10).

**vhratio** - The distance from the tube's center to the vane tips divided by the average helix radius (See Figure 3-9)

**shratio** - ratio of the shell's inner radius to the average helix radius (See Figure 3-9)

**helix_cond** - the effective electrical conductivity of the helix.

The RF signal travels over the surface of the helix structure. The more rough the helix's surface, the longer the wave effectively must travel. The longer the travel, the less effective electrical conductivity. Therefore both the surface roughness and the material's ideal conductivity are indirectly taken into account.

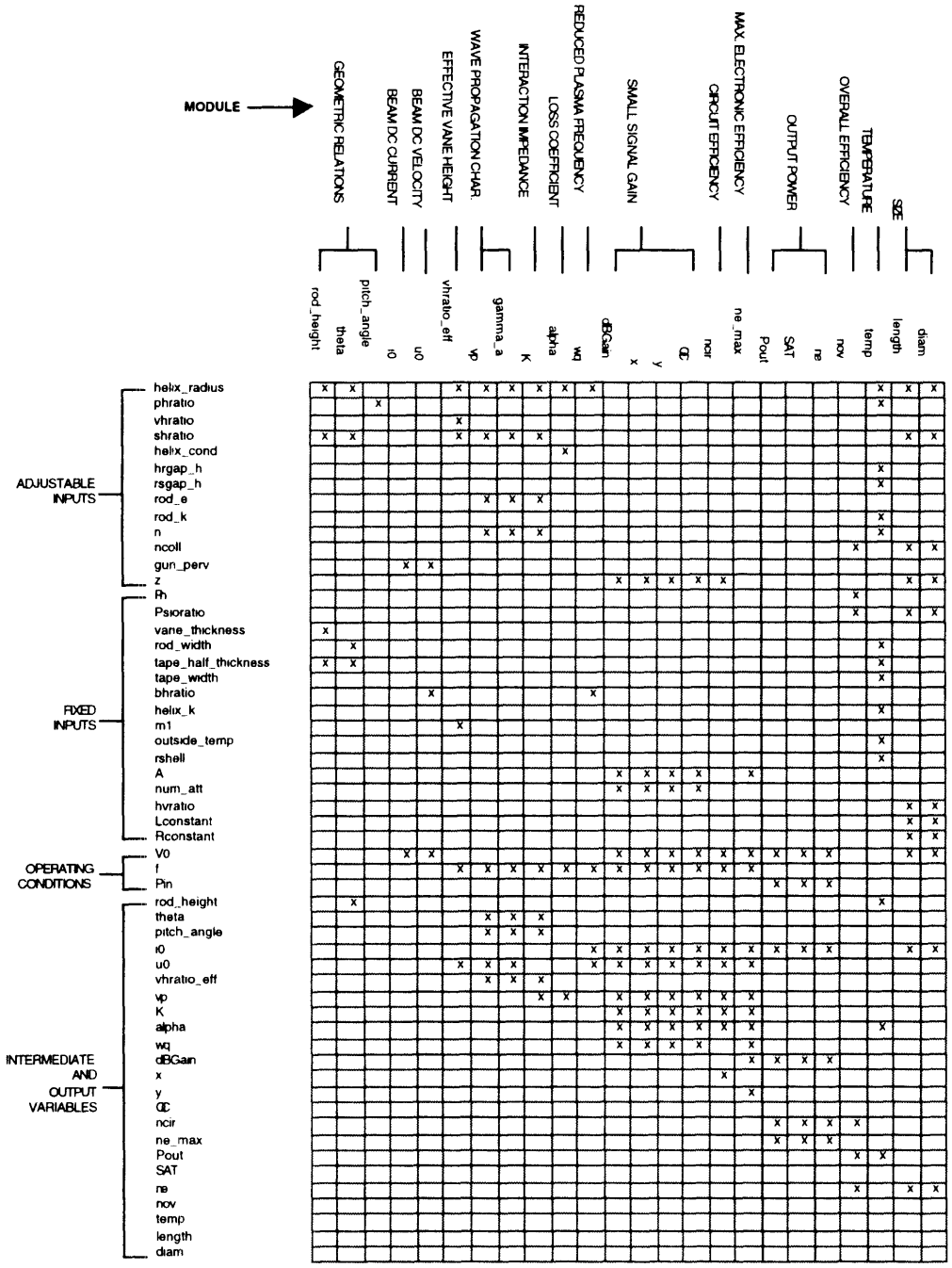


Figure 3-8: Key Variables in the Model and Their Connections

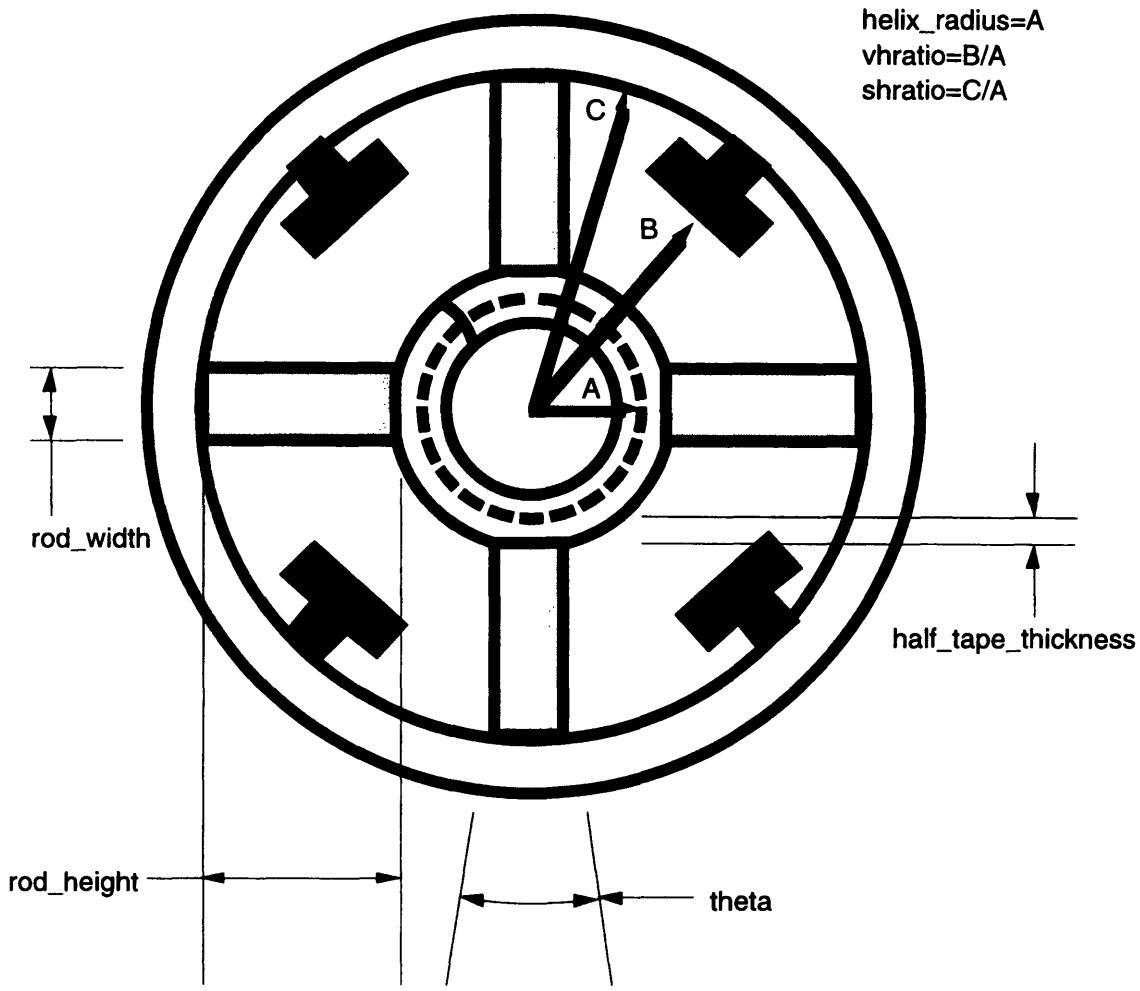


Figure 3-9: Cross Section of TWT Denoting the Various Input Parameters

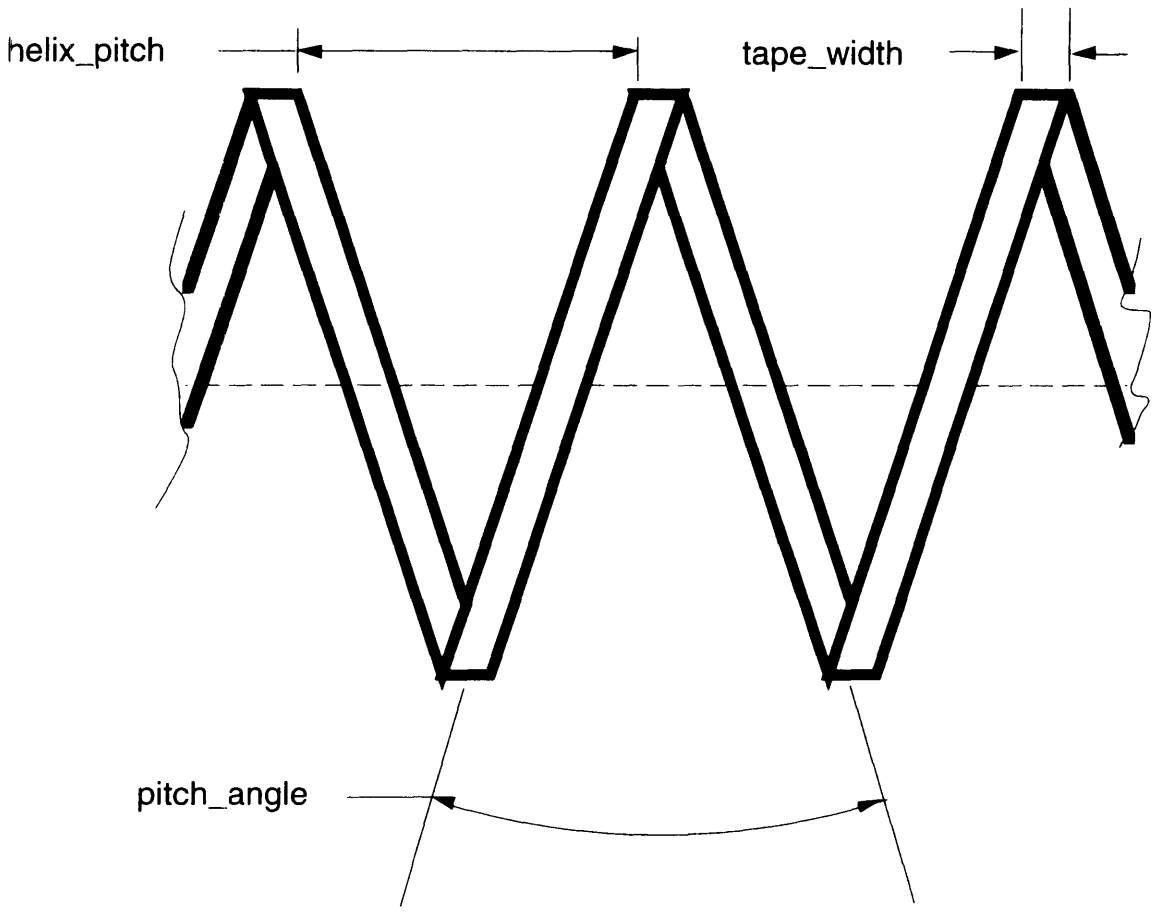


Figure 3-10: Side View of Helix Denoting Various Input Parameters

**hrgap_h** - the thermal gap conductivity between the helix and the support rods

**rsgap_h** - the total thermal gap conductivities between the support rods and the shell

**rod_e** - the relative dielectric constant of the support rods

**rod_k** - the thermal conductivity of the support rods

**n** - the number of rods supporting the helix

**ncoll** - the collector's efficiency in recouping the beam's spent energy

**gun_perv** - the perveance of the gun

It is a single parameter that summarizes the gun's designs influence on the beam's current.

**z** - the length of the helix over which the interaction between the beam and RF wave occurs

### 3.4.2 Fixed Design Parameters

The following is list of design parameters that are fixed in the model. They cannot be altered by the tool's user or search routine.

**Ph** - power required to run the heater

**Psioratio** - ratio of beam power intercepted by helix or absorbed by harmonics to the beam's power

**vane_thickness** - thickness of the loading vanes

**rod_width** - average width of the support rods (See Figure 3-9)

**tape_half_thickness** - half radial thickness of the helix (See Figure 3-9)

**tape_width** - axial width of helix (See Figure 3-10)

**bhratio** - ratio of the beam's radius to the helix's average radius

**helix_k** - thermal conductivity of the helix

**n_v** - number of vane tips

**op_temp** - temperature of the unpackaged TWT's environment

**rshell** - combined thermal resistance of the shell, magnets, and pole pieces

**A** - gain loss parameter

Attenuators are placed within the TWT to eliminate back propagation of the RF signal due to impedance mismatches. This parameter measures the reduction in gain because of these attenuators.

**hvratio** - measures the ability of the collector to absorb heat per cubic meter

**Lconstant** - length of objects within the TWT not modeled (i.e. the gun)

**Rconstant** - thickness of unmodeled objects within the TWT that contribute to its total radius (i.e. magnets and pole pieces).

### 3.4.3 Operating Parameters

These variables describe the operating conditions under which each TWT is expected to meet the specifications. They are similar to specifications in that they cannot be changed by the designer.

**V0** - the voltage applied at the cathode

**f** - the frequency of the incoming RF signal

**Pin** - the power of the incoming RF signal

### 3.4.4 Performance Parameters

These are the outputs of the model. They must meet the specifications set by the MPM integrators.

**SS Gain** - the small signal gain of the TWT

Gain is the ratio of the RF signal's power upon entering the tube to its power when leaving. If the TWT is far from saturated (and therefore the gain small), this parameter is constant as input power changes.

**Pout** -the power within the RF signal leaving the tube

**temp** - the hottest temperature within the helix structure during operation

**nov** - the overall efficiency of the TWT

This parameter compares the useful power within the amplified RF signal to the total power used to produce it.

**length** - the total length of the unpackaged TWT

**diam** - the total diameter of the unpackaged TWT

**i0** - the DC current of the electron beam

### 3.4.5 Geometric Relations Module

**inputs**

helix_radius, phratio, vhratio, shratio, vane_thickness, rod_width, tape_half_thickness, vane_height

**outputs**

**rod_height** - radial length of the supporting rod (See Figure 3-9)

**theta** - average degree of coverage of each of the supporting rods (See Figure 3-9)

**pitch_angle** - pitch angle of helix (See Figure 3-10)

**equations**

$$rod\_height = helix\_radius \bullet (shratio - 1) - vane\_thickness \tag{3-1}$$

$$theta = \frac{360 \bullet rod\_height \bullet rod\_width}{\pi \bullet (helix\_radius \bullet shratio)^2 - \pi \bullet (helix\_radius + tape\_half\_thickness)^2} \tag{3-2}$$

$$pitch\_angle = \frac{180}{\pi} \arctan\left(\frac{phratio}{2 \bullet \pi}\right) \tag{3-3}$$

**description**

The module contains a series of geometric relations. Both the pitch_angle and theta equations convert inputted or fixed design parameters into metrics used by other modules. The rod_height relation represents the constraint that the rod must be connected to the helix and the shell.

Figure 3-11 shows a tapered helix. The tapering of the pitch angle can offer higher small signal gain and overall efficiency. The geometry cannot be handled by the model. However, the real limitation stems not from the geometry module but from the module which calculates small signal gain. Later modules require a description of the TWT geometry in simple, gross terms (as will be shown). Therefore, the geometric equations in this module tend to be approximations or averages. Improvement in this module would first require the improvement of others.

### 3.4.6 Beam DC Current Module

**inputs**

gun_perv, V0

**outputs**

i0

**equations**

$$i0 = gun\_perv \bullet V0^{3/2} \tag{3-4}$$

where the above equation was taken from [Gilmour, 1994].

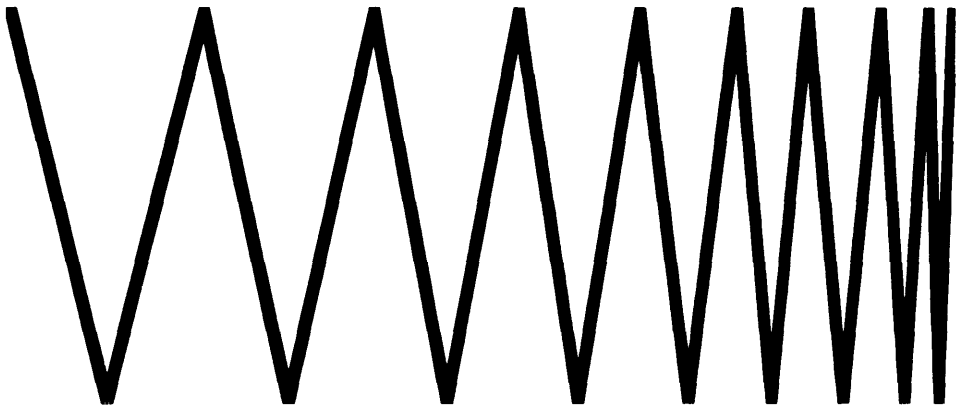

Figure 3-11: Schematic of a Tapered Helix

**description**

As electrons emerge from the heated cathode, they are accelerated by the applied voltage to form the electron beam. Increases in the electron emission rate ( by increasing the cathode temperature for example) will have no effect on the beam's current. Since electrons have negative charge, their emission from the cathode depresses the voltage potential near the cathode to a negative value. Electrons are essentially repelled back into the cathode. Therefore, only raising the applied potential can increase the beam's current. TWT's produced at the manufacturer have this trait. The potential can be altered by adjusting either the operation voltage (V0) or the geometry of the control electrodes that form the beam. The gun's perveance captures the net effect of the changing the latter . The equation does not directly describe the influence of the gun's geometry. The perveance in the TWT studied is easily changed through a series of screw adjustments from 4.5 to 5.7 E-6 pervs. A perveance beyond this range requires a redesign of the gun's geometry. Modeling the gun's geometry would provide the user with a greater range of perveance values to choose from.

### 3.4.7 Beam DC Velocity Module

**input**

gun_perv, V0

**output**

**u0** - the average velocity of the electrons moving in the beam

**equations**

$$Veff = V0 \bullet \left(1 - gun\_perv \bullet \frac{(1 - 2 \bullet \log(bhratio))}{4\pi \bullet e0\sqrt{2 \bullet nu}}\right) \tag{3-5}$$

$$u0 = c \bullet \sqrt{1 - \left(1 + \frac{Veff}{Vn}\right)^{-2}} \tag{3-6}$$

where e0, nu, Vn, and c are constants equal to $8.85 \bullet 10^{-12}$, $1.76 \bullet 10^{11}$, $5.11 \bullet 10^{8}$, *and* $3 \bullet 10^{8}$ respectively. All equations are from [Gilmour, 1994].

**description**

The applied voltage maintains the electron beam at an average velocity. Equation 3-6 describes this phenomenon, including relativistic effects. However, the equation does not consider the rotational velocity experienced by the electrons. As mentioned before, a magnetic field is applied to the beam to prevent it from expanding. Initially, an electron traveling down the tube is exposed to a radial magnetic field. Lorentz's Law ( $F = -e \bullet (E + u \times B)$ ) requires that a tangential force be applied to the electron. The electron begins to acquire a circumferential velocity component. The rotational velocity then causes the electron to cut across the axial flux lines as it travels further down the tube. An inward radial force results, just balancing the combined repulsive and centrifugal forces at a specified beam radius. These facts explain how the magnets prevent the beam from expanding. As a side effect, the electrons' axial velocities becomes somewhat reduced due to their rotational energies. Equation 3-5 reduces the voltage inserted into equation 3-6 to account for the rotational energy.

Most analyses of electron beams in the literature, including the above equations, assume laminarity in the flow. In laminar flow, electrons trajectories do not cross. This assumption greatly simplifies the analysis. In addition, ion effects are typically ignored. The vacuum within a TWT is not perfect. Ions become trapped within the beam, reducing the repulsive forces and increasing the effective voltage. A.S. Gilmour [Gilmour, 1994] discusses these phenomena and offers theory developed by Richard True for dealing with non-laminar flow. Use of his work may yield more accurate predictions.

### 3.4.9 Effective Vane Height Module

**input**

helix_radius, vhratio, shratio, w, u0

**output**

**vhratio_eff** - the effective vhratio

vhratio_eff is a modification of the true vhratio to improve the modeling of the vane's influence on the propagation characteristics of the wave in later modules.

**equations**

$$d = shratio \bullet helix\_radius \bullet gamma \tag{3-7}$$

$$b = vhratio \bullet helix\_radius \bullet gamma \tag{3-8}$$

$$r = vhratio\_eff \bullet helix\_radius \bullet gamma \tag{3-9}$$

$$\frac{K(4,r) \bullet I(4,d) - K(4,d) \bullet I(4,r)}{K(4,b) \bullet I(4,d) - K(4,d) \bullet I(4,b)} = 0.55 \tag{3-10}$$

where K(x,y) and I(x,y) are the modified Bessel functions of order x of the first and second k kind respectively with y as their argument and gamma is the axial propagation constant of RF wave. Equation 3-10 was taken from [Kumar et. al., 1989].

**description**

The analytical equations used in the module that determines the propagation characteristics of the RF signal assume simplified geometries for the support rods and metal vanes. The vanes are assumed to be a series of infinitely thin, infinitely many fins extending from the shell. Figure 3-12 shows this simplified view. In the simplified model, the axial electric field completely vanishes at the fin's tips, but the azimuthal electric field extends to the shell's surface. In reality, the field extends beyond the vanes tips due to the true spacing between them (See Fig 3-9). Equation 3-10 compares the strength of the axial field at an arbitrary radius in the inter-vane region to that at the vane's tips. As r increases in this region, the field decreases. The axial field's extension can be accounted for by decreasing the height of the vanes (increasing the vhratio) entered into the wave propagation module. [Kumar et. al., 1989] have found that the effective vhratio is equal to r/helix_radius where r is the radius that reduces the field strength to 55% of the value found at the vane's tips.

This detailed modeling of the vane was deemed necessary due its great influence of small signal gain. A 1% change in the vane height can alter the small signal gain by 1 dB. Many simulations used by industry do not model the vane at this level of detail. The need for better modeling of the vanes was one of the primary reasons why industrial simulations were not used.

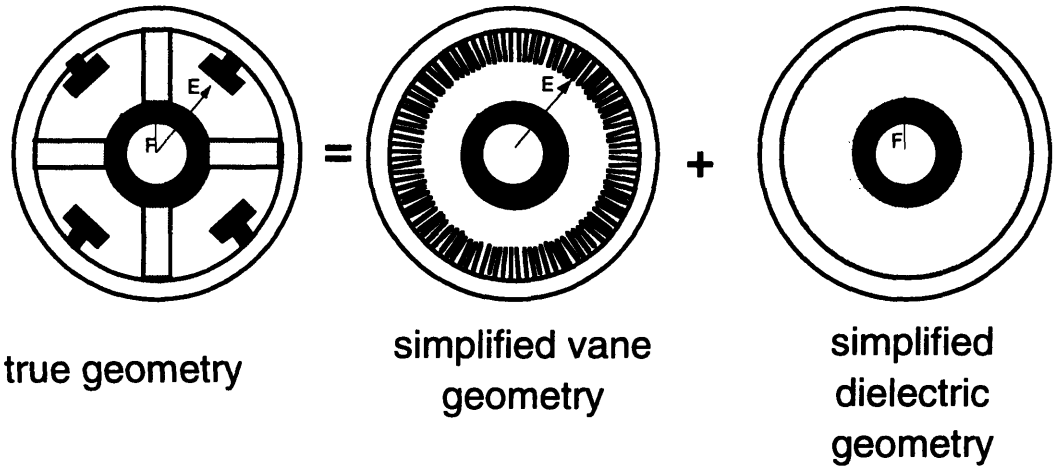


Figure 3-12: Simplified Model Used by Propagation Characteristic and Interaction Impedance Modules

Several difficulties were overcome in order to program this module. Although MATLAB, the programming environment used to construct the model, has the capability to calculate the modified Bessel functions I(x,y) and K(x,y), no commands exist to find their inverse. Therefore, numerical methods were used to determine r. The actual vane height was used as a good starting guess.

Under the MATLAB environment, the calculation times of the Bessel functions were long. Matrices "Tbesseli" and "Tbesselk" were created which function as look-up tables. Use of the look-up tables reduced the calculation time by roughly a factor of ten.

Gamma, the radial propagation constant of the wave, is an input into this module. Gamma cannot be determined until the effective vhratio is found. The above equations and those used to find gamma form a set of simultaneous equations. These equations could be simultaneously solved to determine both gamma and vhratio exactly. However, the iterations would significantly slow down the run time of the model. Vhratio_eff is not sensitive to gamma. A fifty percent change in gamma typically changes vhratio_eff by a value less than one percent. An excellent approximation to gamma is w/u0. This approximation was used to reduce the computational expense of running the model.

### 3.4.10 Wave Propagation Characteristics Module

**input**

helix_radius, pitch_angle, vhratio_eff, shratio, rod_e, theta, n, u0, w

**output**

**gamma** - the cold circuit, radial propagation constant of the wave. The radial propagation constant of the RF signal if the beam were not present.

**vp** - the cold circuit, axial velocity of the wave. The axial velocity the wave would travel at if the electron beam were not present.

**equations**

$$a = helix\_radius \bullet gamma \tag{3-11}$$

$$e_{eff} = 1 + (rod\_e - 1) \bullet \frac{n \bullet theta}{360} \tag{3-12}$$

$$G = K(0,a) \bullet K(1,a) \bullet \left[ e_{eff} \bullet \left( 1 + \frac{I(1,a) \bullet K(0,b)}{K(1,a) \bullet I(0,b)} \right) - \left( 1 - \frac{I(0,a) \bullet K(0,b)}{K(0,a) \bullet I(0,b)} \right) \right] \tag{3-13}$$

$$H = -K(1,a) \bullet I(0,a) \bullet e_{eff} \bullet \left( 1 + \frac{I(1,a) \bullet K(0,b)}{K(1,a) \bullet I(0,b)} \right) - I(1,a) \bullet K(0,a) \bullet \left( 1 - \frac{I(0,a) \bullet K(0,b)}{K(0,a) \bullet I(0,b)} \right) \tag{3-14}$$

$$\alpha_C = \left( 1 + \frac{I(0,a) \bullet G}{K(0,a) \bullet H} \right)^{-1} \tag{3-15}$$

$$\alpha_L = \left( 1 - \frac{I(1,a) \bullet K(1,d)}{K(1,a) \bullet I(1,d)} \right) \tag{3-16}$$

$$D = (\alpha_C \bullet \alpha_L)^{-0.5} \tag{3-17}$$

$$gamma = \frac{w \bullet \cot(pitch\_angle)}{c \bullet D} \bullet \left( \frac{I(0,a) \bullet K(0,a)}{I(1,a) \bullet K(1,a)} \right)^{-0.5} \tag{3-18}$$

$$vp = w \bullet \left( gamma^2 + \left( \frac{w}{c} \right)^2 \right)^{-0.5} \tag{3-19}$$

where b and d are as defined in equations (3-8) and (3-7) respectively (except vhratio_eff replaces vhratio) and c is the speed of light. All equations are based upon [Kumar et. al., 1989].

**description**

The equations are essentially field solutions capturing the effect of the supporting rods, vanes, shell, and helix on the electric and magnetic fields within the TWT. As mentioned above, the analysis behind these equations assumes the simplified geometry presented in Figure 3-12.

Although the vhratio inputted into the model has been adjusted to account for the axial field's extension, the model still represents an

approximation to the true spatial distribution of the electric field in the tube. Much more accurate approaches exist. For instance, [Kumar et. al., 1989] mentions work by Kravchenko [Kravchenko, 1976]. The manufacturer uses a model to calculate vp that takes into account the tape width of the helix. More detailed analyses would improve the overall model's accuracy as gain is extremely sensitive to changes in the cold circuit velocity. A 1% change in the cold circuit velocity can result in a 2 dB change in gain.

### 3.4.11 Interaction Impedance Module

**input**

vp, helix_radius, vhratio_eff, shratio, pitch_angle, rod_e, theta, n, w

**output**

**K** - the interaction impedance

This parameters describes the strength of the coupling between the beam and RF signal's electric and magnetic fields.

**equations**

$$Xad = \frac{I(1,a) \bullet K(1,d)}{I(1,d) \bullet K(1,a)} \tag{3-20}$$

$$Eta = \frac{I(0,a) \bullet K(0,b)}{K(0,a) \bullet I(0,b)} \tag{3-21}$$

$$F1 = \frac{\beta \bullet w \bullet e0}{gamma^2 \bullet (1 - Eta)^2} \tag{3-22}$$

$$F2 = \frac{\beta \bullet \tan\left(pitch\_angle \bullet \frac{\pi}{180}\right)^2}{w \bullet mu0 \bullet (1 - Xad)^2} \tag{3-23}$$

$$V7 = -2 \bullet F2 \bullet Xad \bullet \frac{I(0,a)^2}{I(1,a) \bullet K(1,a)} \tag{3-24}$$

$$V6 = F2 \bullet \left(\frac{I(0,a)}{K(1,a)}\right)^2 \tag{3-25}$$

$$V5 = F2 \bullet Xad^2 \bullet \left(\frac{I(0,a)}{I(1,a)}\right)^2 \tag{3-26}$$

$$V4 = 2 \bullet F1 \bullet e_{eff} \bullet Eta \bullet \left( \frac{I(0,a)}{K(0,a)} \right) + V7$$

(3-27)

$$V3 = F1 \bullet e_{eff} \bullet \left( \frac{I(0,a)}{K(0,a)} \right)^2 + V6$$

(3-28)

$$V2 = F1 \bullet e_{eff} \bullet Eta^2 + V5$$

(3-29)

$$V1 = \frac{\beta \bullet w \bullet e0}{gamma^2} + \frac{\beta}{w \bullet mu0} \bullet \left( \frac{I(0,a)}{I(1,a)} \right)^2 \bullet \tan\left( pitch\_angle \bullet \frac{\pi}{180} \right)$$

(3-30)

$$Q(x) = 0.5 \bullet \left( \frac{x}{gamma} \right)^2 \bullet \left[ \left( I(0,x) \bullet K(0,x) + I(1,x) \bullet K(1,x) \right) + x^{-1} \bullet \left( I(0,x) \bullet K(1,x) - I(1,x) \bullet K(0,x) \right) \right]$$

(3-31)

$$P2(x) = -0.5 \bullet \left( \frac{x}{gamma} \right)^2 \bullet K(0,x) \bullet K(1,x) \bullet \left( \frac{K(0,x)}{K(1,x)} - \frac{K(1,x)}{K(0,x)} + \frac{2}{x} \right)$$

(3-32)

$$P1(x) = 0.5 \bullet \left( \frac{x}{gamma} \right)^2 \bullet I(0,x) \bullet I(1,x) \bullet \left( \frac{I(1,x)}{I(0,x)} - \frac{I(0,x)}{I(1,x)} + \frac{2}{x} \right)$$

(3-33)

$$U7 = \int_{b/gamma}^{d/gamma} I(1, x \bullet gamma) \bullet K(1, x \bullet gamma) \bullet x \bullet dx = Q(a) - Q(b)$$

(3-34)

$$U6 = \int_{b/gamma}^{d/gamma} K(1, x \bullet gamma)^2 \bullet x \bullet dx = P2(d) - P2(b)$$

(3-35)

$$U5 = \int_{b/gamma}^{d/gamma} I(1, x \bullet gamma)^2 \bullet x \bullet dx = P1(d) - P1(b)$$

(3-36)

$$U4 = \int_{a/gamma}^{b/gamma} I(1, x \bullet gamma) \bullet K(1, x \bullet gamma) \bullet x \bullet dx = Q(b) - Q(a)$$

(3-37)

$$U3 = \int_{a/gamma}^{b/gamma} K(1, x \bullet gamma)^2 \bullet x \bullet dx = P2(b) - P2(a)$$

(3-38)

$$U2 = \int_{a/gamma}^{b/gamma} I(1, x \bullet gamma)^2 \bullet x \bullet dx = P1(b) - P1(a) \tag{3-39}$$

$$U1 = \int_{0}^{a/gamma} I(1, x \bullet gamma)^2 \bullet x \bullet dx = P1(a) \tag{3-40}$$

$$K = \left(2 \bullet \beta^2 \bullet \pi \sum_{i=1}^{7} Ui \bullet Vi\right)^{-1} \tag{3-41}$$

where a, b, and d are as defined previously, x is a dummy variable, mu0 is a constant equal to $4 \bullet \pi \bullet 10^{-7}$, and β is equal to w/vp. All equations were taken from [Kumar et. al., 1989].

**description**

K measures the strength of the wave's electric field within the region occupied by the electron beam. Large field values correlate with tight bunching of the beam during its interaction with the RF signal. High gains per axial inch of the helix thus coincide with large K values. K decreases with increasing frequency. At high frequencies, the number of helix turns per wave length decreases. The electric field falls off more rapidly as one moves away from the helix tape. Variables that influence the radial electric field, such as gamma or loading factors like vhratio_eff, will also influence K.

The same limitations mentioned in the wave propagation model due to the simplified geometry apply here as both draw upon the same analysis. However, K does not have such a large effect on gain as velocity does. Also, the beam's diameter and radial density distribution are neglected. The closer the electrons in the beam are to the helix tape, the higher the interaction impedance.

During the computer implementation of these equations, two typographical errors where found in the literature. The signs in front of P2(x) were reversed. With the mistype, the integrals U3 and U6 were reporting negative values. The integrand K(x,y)^2 * r in equations 3-35 and 3-38 are always positive. Therefore, P2(d) > P2(b) > P2(a) if d > b > a. This contradicts the results initially obtained using this module.

Numerical integration of equations 3-35 and 3-38 were performed to calculate U3 and U6 instead of using P2(x). The results matched those provided by [Kumar et. al., 1989]. In this way, the error was found as the

numerical integrations of U3 and U6 were the exact negatives of their mistyped, closed form counterparts.

### 3.4.12 Loss Coefficient Module

**input**

w, vp, helix_radius, helix_cond

**output**

**alpha** - loss coefficient of the helix

Alpha is defined as Pl/2Pt where Pl is the power lost due to resistance per meter as Pt units of power travels through the helix.

**equations**

$$F1 = 1 + \exp\left(2.601 - 1.268 \bullet w/vp \bullet helix\_radius\right) \tag{3-42}$$

$$ds = \left(0.2 \bullet w \bullet mu0 \bullet helix\_cond\right)^{-0.5} \tag{3-43}$$

$$alpha = \left(\frac{w}{vp}\right)^2 \bullet \frac{ds}{2} \bullet F1 \tag{3-44}$$

where all equations were taken from [Rowe, 1965].

**description**

As the wave propagates down the tube, electrons in the helix, tube, vanes, and rods oscillate in response. These oscillations face resistance in their respective materials causing part of the wave's energy to be lost and converted into heat. The above set of equations only model the loss due to the helix material.

[Gilmour, 1979] performs a more detailed analysis which includes loss contributed by the dielectric rods and shell. Loading vanes, however, are not considered. Use of his model would increase the ability to predict alpha accurately, although his observations report that the helix accounts for over 80% of the loss within the helix. These findings were backed by his experimental results.

Gilmour discovered that the helix surface roughness has a large effect on the effective conductivity (helix_cond) of the helix. Both Gilmour's analysis and the one presented in this module do not directly capture the

effect of surface roughness. Such a connection would be useful to more closely examine new helix polishing techniques.

### 3.4.13 Reduced Plasma Frequency Module

**input**

helix_radius, bhratio, i0, u0, w, Veff

**output**

**wq**- the reduced plasma frequency

As the electrons become bunched in the beam, repulsion forces build between them. A series of waves are set up similar to those in acoustics. The natural oscillation of the electrons in these waves given that the beam is of finite diameter is termed the reduced plasma frequency.

**equations**

$$beam\_radius = bhratio \bullet helix\_radius \tag{3-45}$$

$$po = \frac{i0}{\pi \bullet u0 \bullet beam\_radius^2} \tag{3-46}$$

$$wp = \sqrt{\frac{nu \bullet po}{e0}} \tag{3-47}$$

$$R = \left(1 + \left(\frac{1.78}{\frac{w}{u0} \bullet beam\_radius}\right)^2\right)^{-0.5} \tag{3-48}$$

$$wq = R \bullet wp \tag{3-49}$$

where all equation were obtained from [Gilmour, 1994].

**description**

The more tightly packed the electrons are before bunching, the higher space charge forces in the beam. Large values for wq result. i0, the beam's diameter (bhratio*helix_radius), and u0 determine the charge density. Electrons in the outer regions of the beam do not experience the same forces as those deep inside the beam. Field analysis is needed to take such phenomena into account. As a result, w is employed along with u0 to determine the propagation constant of the beam as it bunches. The bunching

strongly affects the fields around the beam and thus the electrons on the outer region of the beam.

Assumptions made in this module are similar to those made in the beam velocity module. More detailed analyses exist, but the ones found require intensive numerical computation [Fanton, 1985] and [Palmer et. al., 1993].

### 3.4.14 Small Signal Gain Module

**input**

K, vp, alpha, u0, i0, Veff, helix_radius, z, w, A, wq

**output**

dBGain

x - a parameter measuring the degree of synchronism between the beam and the wave

y - a measure of the propagation constant of the RF wave relative to the beam's

**equations**

$$C = \left(\frac{K \bullet i0}{4 \bullet V0}\right)^{1/3} \tag{3-50}$$

$$QC = \left(\frac{wq}{2 \bullet C \bullet w}\right)^2 \tag{3-51}$$

$$b = \frac{1}{C} \bullet \frac{u0 - vp}{vp} \tag{3-52}$$

$$d = \frac{alpha}{C \bullet \frac{w}{vp}} \tag{3-53}$$

$$del^2 = \frac{\left(1 + b \bullet C - j \bullet C \bullet d\right) \bullet \left(1 + b \bullet C\right)^2}{\left(-b + j \bullet del + j \bullet d\right) - 0.5 \bullet C \bullet \left(del^2 + \left(b - j \bullet d\right)^2\right)} - 4 \bullet QC \tag{3-54}$$

$$x = \mathrm{Re}(del) \tag{3-55}$$

$$y = \mathrm{Im}(del) \tag{3-56}$$

$$dBGain = 2 \bullet A + 54.6 \bullet x \bullet C \bullet z \bullet \frac{w}{u0 \bullet 2 \bullet \pi} - 6 \tag{3-57}$$

where j is equal to the square root of negative one and all equations were taken from [Srivastava and Joshi, 1993].

**description**

The original approach of this derivation dates back to the 1950's with J.R. Pierce [Pierce, 1950]. The equations capture the beam-wave interaction described earlier. The wave induces the beam to bunch; the bunched beam amplifies the wave. C, proportional to K, captures the strength of the coupling between the beam and wave. b compares vp to u0. To maximize the growth rate of the beam, the actual velocity of the RF signal slightly lags that of the beam's. Such a velocity correlates with a b value from -2 to 4 depending on QC. QC is a ratio comparing wq to C. Through QC, space charge forces come into play. The stronger the space charge forces, the greater the optimal b value. Alpha drives d, a parameter which reduces gain to account for circuit loss. The longer the helix, the more time the electron beam and wave interact. Since the amplification effect occurs over each wavelength, the higher the frequency the more amplification "cycles." Finally, A subtracts dB due to the attentuators.

The above equations only work when the amplification of the wave is "small." Thus, the term small signal gain. In fact, the whole theory behind the equations is called small signal theory. Fundamentally, equations 3-50 through 3-57 come from solving Maxwell's equations for the beam and the wave. Differential equations inevitably come into play which are easily solved by assuming a sinusoidal solution and eliminating small, nonlinear terms. These assumptions cannot be made when the gain of the tube nears its saturation level. Figure 3-13 shows the "large signal region." Theory has been developed to deal with such nonlinearities. More sophisticated beam analysis (than is presented here) could be incorporated into the model to deal with the complex, non sinusoidal behavior that occurs in the beam. A set of partial, nonlinear differential equations could capture the large signal beam-wave interaction [Rowe, 1965]. Simulations have been developed which numerically solve these equations [Fanton, 1985] and [Palmer, et. al., 1993]. The manufacturer studied had such simulation software. The program took 20 minutes to run. The current model follows over 20 discrete electron charge groups in the beam during the interaction. Perhaps this number could be reduced without excessively sacrificing model accuracy.

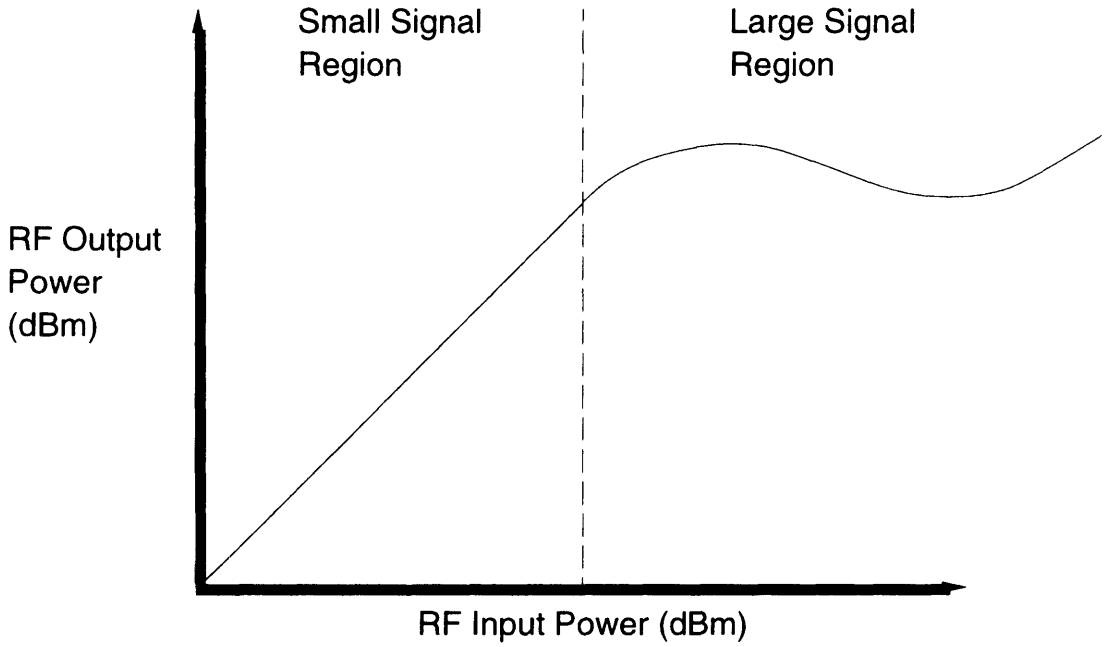


Figure 3-13: Curve Depicting Difference Between Large and Small Signal Regions of TWT

### 3.4.15 Circuit Efficiency Module

**inputs**

K, i0, V0, x, w, vp, alpha, u0, z

**outputs**

**ncir** - the circuit efficiency of the helix.

This parameter measures how effectively the helix transmits the RF wave's power.

**equations**

$$C = \left(\frac{K \bullet i0}{4 \bullet V0}\right)^{1/3} \tag{3-58}$$

$$B = 54.6 \bullet x \tag{3-59}$$

$$N = z \bullet \frac{w}{vp \bullet 2 \bullet \pi} \tag{3-60}$$

$$PltoPout = \frac{alpha}{C \bullet x \bullet \frac{w}{u0}} \bullet \left(1 - \exp\left(-2 \bullet B \bullet C \bullet N\right)\right) \tag{3-61}$$

$$ncir = \left(1 + PltoPout\right)^{-1} \tag{3-62}$$

**description**

At every point along the central axis of the tube, the power lost per axial length can be calculated using the input parameters above. By integrating over the entire axial length, the ratio between the total power lost and power out can be ascertained to determine ncir.

### 3.4.16 Maximum Electronic Efficiency Module

**inputs**

dBGain, w, wq, K, i0, Veff, u0, vp, alpha, A, y

**outputs**

**ne_max** - the maximum efficiency provided by the tube.

**equations**

$$C = \left(\frac{K \bullet i0}{4 \bullet V0}\right)^{1/3} \tag{3-63}$$

$$QC = \left(\frac{wq}{2 \bullet C \bullet w}\right)^2 \tag{3-64}$$

$$b = \frac{1}{C} \bullet \frac{u0 - vp}{vp} \tag{3-65}$$

$$d = \frac{alpha}{C \bullet \frac{w}{vp}} \tag{3-66}$$

$$g = 0.5 \bullet \left(\frac{wq}{C \bullet w}\right)^2 \tag{3-67}$$

$$ne\_\max = 0.75 \bullet (2.75 + 2.42 \bullet b) \bullet (C - 1.85 \bullet C^2) \bullet \left(1 - \frac{g}{53}\right) \bullet (1 + 5 \bullet d + 25 \bullet d^2)^{-1} \tag{3-68}$$

if b<= 1.8 and d<=0.5 else

$$ne\_\max = -2 \bullet C \bullet y \tag{3-69}$$

where equations 3-67 and 3-68 were taken from [Arnett et. al., 1973].

**description**

The equations curve fit the results of several computer simulations, allowing a closed form equation for maximum efficiency. Parameters C, b, QC, and d play similar roles as before. At large signal levels near saturation, the electrons are decelerated so violently and the bunch is so concentrated that another bunch of electrons forms behind the first one. The new bunch begins to grow, drawing electrons from the first one as the gain is increased. The lagging bunch steals energy from the wave. Saturation occurs when the number of electrons in the first bunch equals those in the second, balancing the energy sent to and removed from the RF signal. The curve fit describes the limits saturation places on efficiency. The curve fit has a finite range of accuracy, however. Outside the range, a lower bound on the efficiency is used

(equation 3-69). The lower bound has been slightly improved through comparison with experimental results [Gilmour, 1994].

The use of the large signal simulations described in [Fanton, 1985] and [Palmer, et. al., 1993] indirectly calculate the maximum efficiency. Maximum efficiency is used in the power module to predict the maximum output power. Large signal models can directly model saturation effects on power, removing the need for this module altogether.

### 3.4.17 Output Power Module

**inputs**

i0, Veff, dBGain, Pin, ne_max, ncir, z

**outputs**

**Pout** - Power in the RF signal leaving the TWT

**SAT**- a measure of whether the TWT is in the saturation region or not. The output power level minus that at saturation.

**equations**

$$Pout\_est = 10^{\frac{dBGain}{10}} \bullet Pin \tag{3-70}$$

$$P0 = i0 \bullet V0 \tag{3-71}$$

$$Pout\_\max = ne\_\max \bullet ncir \bullet P0 \tag{3-72}$$

$$SAT = Pout\_est - Pout\_\max \tag{3-73}$$

$$Pout = \min\left(Pout\_est, Pout\_\max\right) \tag{3-74}$$

$$ne = \frac{Pout}{P0 \bullet ncir} \tag{3-75}$$

**description**

These equations are fairly simple, representing basic power relations. One thing to note: the program does limit the power level to the saturation level if the small signal gain equation unknowingly predicts a power level beyond the saturation point.

Once again the issue of accuracy limits are important. The small signal gain module can be used to calculate output power, but only for those values below the saturation level. The module causes a distinct "knee" in the power curve as opposed to the smooth transition that truly occurs. This could be improved by using large signal techniques.

Harmonic power is also ignored. Not only does the primary frequency signal become amplified, but the harmonics that arrived with the incoming signal increase. The power absorbed in these harmonics is effectively lost. In addition, the harmonics impact the central frequency's interaction with the beam, further reducing the usable output power. All these effects can be taken into account by using large signal analysis.

As the amplified signal exits the TWT, it passes through a thin piece of dielectric material. This "window" is needed to insure the vacuum environment within the TWT. However, mismatches in the impedance between the output connecting cable, the window, and the wiring in the helix result in some back reflection. This reflection is not significant enough to interfere with the beam-wave interaction due to the attentuators. However, a measurable amount of power can be lost during the transition. Variations in the geometry of this window influence its impedance and therefore the power out. This whole area of the TWT's design was not studied in the model. Basic microwave transfer line theory could be employed to obtain a rough estimate of the window's influence on power.

### 3.4.18 Overall Efficiency Module

**inputs**

i0, Veff, Pout, ncir, ncoll, Psioratio

**outputs**

**nov** - overall efficiency of the tube

**equations**

$$P0 = \frac{Pout}{ncir \bullet ne} \tag{3-76}$$

$$nov = \frac{ncir \bullet ne}{\frac{Ph + P0}{P0} - ncoll \bullet \left(1 - ne - Psioratio\right)} \tag{3-77}$$

where both equations were taken from [Gilmour, 1994].

**description**

The beam's average current and voltage describe its power. The useful microwave power leaving the TWT vs. that power entering it provide an estimate of the efficiency of the beam-wave interaction. The collector's efficiency determines the power recovered from the spent beam and Psioratio captures power lost due to harmonic effects. Finally, power sent to the heater to generate the beam is accounted for in Ph. The equation merely accounts for all power flows within the tube to find the ratio of flow out to flow in.

### 3.4.19 Temperature Module

**inputs**

helix_radius, phratio, helix_k, rod_width, rod_k, rsgap_h, tape_width, tape_half_thickness, rshell, Pout, alpha, outside_temp

**outputs**

**temp** - hottest temperature on the helix

**equations**

$$helix\_thickness = 2 \bullet helix\_half\_thickness$$

(3-78)

$$Q = 2 \bullet Pout \bullet alpha \bullet \frac{helix\_pitch}{2 \bullet n}$$

(3-79)

$$a = \frac{helix\_pitch}{2}$$

(3-80)

$$b = \frac{helix\_pitch - helix\_width}{2}$$

(3-81)

$$w = rod\_height$$

(3-82)

$$L = \frac{1}{n} \bullet \pi \bullet helix\_radius$$

(3-83)

$$d = \frac{rod\_width}{2}$$

(3-84)

$$Bi = \frac{rsgap\_h \bullet a}{rod\_k}$$

(3-85)

$$sum = \sum_{i=1}^{\infty} \left[ \frac{0.5 \bullet \sin\left(2 \bullet i \bullet \pi \bullet \frac{b}{a}\right)}{i^2} \bullet \frac{\cosh\left(i \bullet \pi \bullet \frac{w}{a}\right) \bullet Bi \bullet \sinh\left(i \bullet \pi \bullet \frac{w}{a}\right)}{\sinh\left(i \bullet \pi \bullet \frac{w}{a}\right) \bullet Bi \bullet \sinh\left(i \bullet \pi \bullet \frac{w}{a}\right)} \right]$$

(3-86)

$$rod\_temp = \left(\frac{a}{rod\_k}\right) \bullet \left(\frac{b}{a \bullet Bi} \bullet \left(1 + Bi \bullet \frac{w}{a}\right) + \frac{2}{\pi^2} \bullet sum\right) \bullet \left(\frac{Q}{d \bullet helix\_width}\right)$$

(3-87)

$$gap\_temp = \frac{1}{hrgap\_h} \bullet \frac{Q}{d \bullet 0.5 \bullet helix\_width}$$

(3-88)

$$helix\_temp = \frac{L}{2 \bullet helix\_k} \bullet \frac{Q}{helix\_width \bullet helix\_thickness}$$

(3-89)

$$shell\_temp = rshell \bullet Q$$

(3-90)

$$temp = helix\_temp + gap\_temp + rod\_temp + shell\_temp + outside\_temp$$

(3-91)

where equation 3-86 is taken from [Vansant, 1983].

**description**

If the temperature gets too high, the helix will distort causing the beam to strike the helix. This destroys the TWT. As power flows through the helix, its resistance steals power from the amplified RF signal. The absorbed energy is heat energy and the helix's temperature is elevated high above ambient levels. Conduction prevails as the main method of transporting this heat. Both [Gilmour, 1994] and [Sauseng, 1978] support the conduction argument. Since the helix exists in a vacuum environment, convection phenomena are not present. Studies done at the manufacturer reveal no significant radiative heat transfer. The heat passes to the support rods, shell, magnets and poles, packaging, and finally, the base plate. Figure 3-14 details this path. The hottest point of the helix lies at its output end where the RF power is greatest. Points "A" in Figure 3-14 are farthest from the rods and therefore are the hottest. Resistances for each of the elements in the path (including the helix) can be derived through their geometry and conductivities. As heat flows

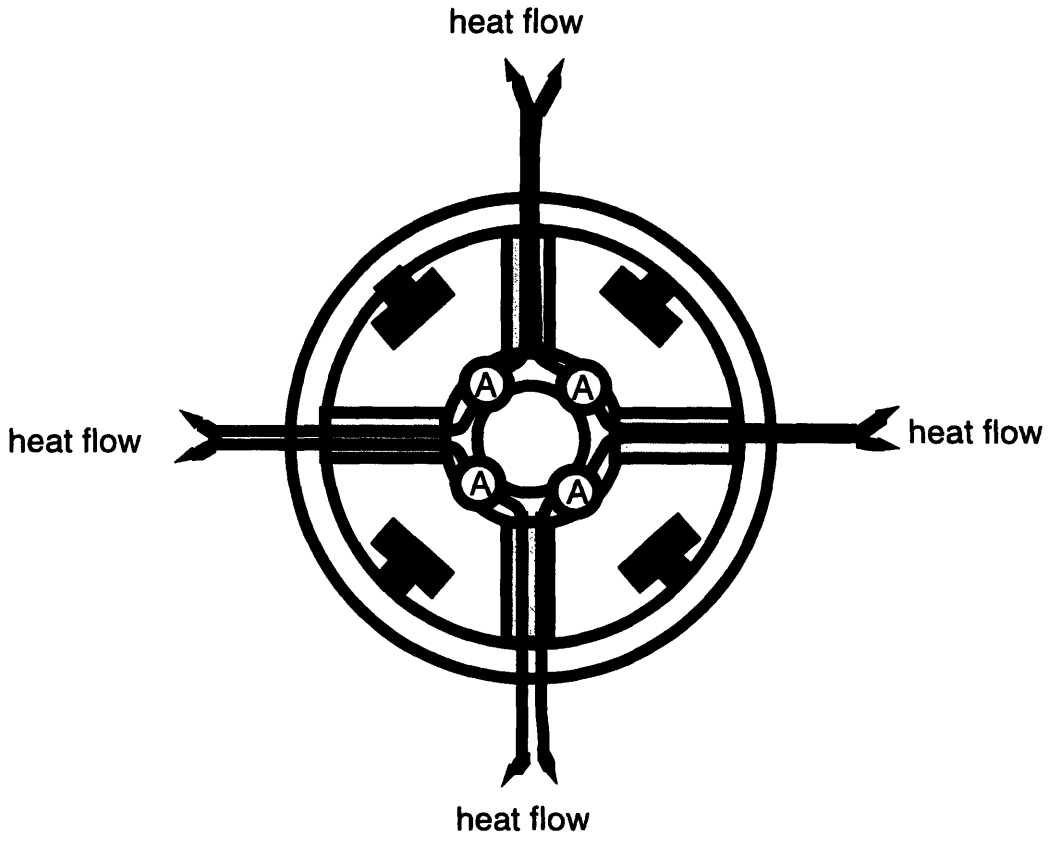


Figure 3-14: Modeled Direction of Heat Flow in TWT

through the thermal path, the total jump in temperature results from multiplying the heat flow by the sum of these resistances.

Thermal models for the TWT could not be found in the literature. The model's basic approach and equations above were derived using the basic theory of heat conduction. Many simplifying assumptions were made during the construction of this model. For example, the heat path was assumed to be the one illustrated in Figure 3-14. Since the helix turns near the input end of the tube carry less power than those towards the output end, this assumption is incorrect. The actual maximum temperature, at the last turn at the output end, is less than predicted as some of the heat is also is conducted down the helix toward the input end. The model is one dimensional; the direction of heat flow is assumed to have no component perpendicular to the path shown in Fig 3-14. Coefficients of heat transfer change with temperature. They were fixed in the model. These and other simplifications do degrade accuracy. Unfortunately, it is difficult to obtain a quantitative feel for the error as empirical data fitting the baseline design could not be found.

### 3.4.20 Size Module

**inputs**

Psioratio, ne, i0, V0, helix_radius, shratio, z, ncoll, Lconstant, Rconstant, hvratio

**outputs**

**diameter** - total diameter of the unpackaged TWT

**length** - total length of the unpackaged TWT

**equations**

$$P0 = i0 \bullet V0 \tag{3-91}$$

$$Rtotal = helix\_radius \bullet shratio + Rconstant \tag{3-92}$$

$$Pspent = P0 \bullet \left(1 - Psiratio - ne\right) \tag{3-93}$$

$$Lcoll = Pspent \bullet \frac{\left(1 - ncoll\right)}{hvratio \bullet 2 \bullet \pi \bullet Rtotal} \tag{3-94}$$

$$length = z + Lconstant + Lcoll \tag{3-95}$$

$$diam = 2 \bullet Rtotal \tag{3-96}$$

**description**

The total diameter varies with changes in the diameter of the shell. Changes in the helix's and collector's length are taken into account to determine the axial length. Helix length is an input variable and does not need to be calculated. The collector's length is dependent upon the wasted power it must absorb. As the spent beam enters the collector, most of its energy is recouped. Some electrons in the beam, however, are not sufficiently decelerated and crash into the collector creating heat. Currently, the collector's volume is considered to be proportional to the amount of heat it can absorb. This is only a rough approximation suggested by the engineer. Better results could be obtained by performing a thermal analysis of the collector. Lconstant and Dconstant represent the sizes of all other components that are not explicitly modeled. They include parts such as the gun assembly for the length calculation and the magnets and pole pieces for the diameter calculation.

## 3.5 Assessment of Model

Admittedly, the model was not directly compared against empirical tests. Good empirical data could not be gleaned from the manufacturer within the time window of the project, though many attempts were made. However, with the exception of the thermal aspects of the TWT, all of equations were taken from the research literature. These equations have already been judged good rough estimates. Nevertheless, a quantitative estimate of the error inherent in the model needs to be ascertained before it is given to industry. There exists a risk that the individual errors of the separate modules could build up making the total error in the estimated performance measures of the tube significant. Fortunately, the primary goal of the thesis project was not seriously compromised. The model captures the basic trends inherent in the tube and can still be used to illustrate the power of the methodology envisioned.

Performance parameters, such as phase shift, are extremely difficult to include. All industry methods for understanding how phase shifts in the RF signal during amplification are related to the various design parameters are computationally intensive. Numerical techniques are used to interactively

solve sets of partial differential equations. Unfortunately, the computational expense demanded by these industry tools prohibit their use in the computer tool developed in this thesis. Many design evaluations need to be conducted to locate the best design. The user simply cannot wait 20 minutes to evaluate a single design point.

Calculations of small signal gain or the maximum efficiency are also rooted in such complex analysis, but much work has been done to simplify their calculation. The result has been the relatively simple analytical formulas used by the model. This simplification process has occurred over a period of years. It cannot be done as part of the model's construction. Finite element methods could have been used to develop to cover all aspects of the tube's thermal behavior, however, the effort would have been a whole thesis project in itself. Use of the optimization framework to predict cost based on performance therefore requires a wealth of past research into the product under study.

# Chapter Four

# Linking Cost and Design to Manufacturing

## 4.1 Overview

This section discusses the relationships that link the TWT's manufacturing process to its design and cost. A brief description of the manufacturing process is provided. Past work in cost estimation, including the industry's current approach, is outlined. This provides the background for the presentation of the approach used in this thesis. Finally, the key pieces of the manufacturing-to-cost and manufacturing-to-design links are presented.

## 4.2 Overview of the Manufacturing Process

Most of the knowledge about the manufacturing process was obtained directly through a visit to the factory floor. All observations were recorded and used to ask further questions in follow-up phone conversations. Slowly, over several weeks, a picture of the major manufacturing activities was constructed.

There are five major sub-assemblies in the TWT produced at the manufacturer: the shell, antenna, anode, collector, and gun. The shell sub-assembly consists of the helix, supports rods, loading vanes, and surrounding metallic shell. The support rods, metal vanes, and helix's tungsten wire are bought from suppliers. The wire is wound on a mandrel to form the helix. Heating and grinding operations are performed to better define the helix's geometric and material properties. Workers coat the support rods with carbon patterns that function as the attenuators. All three major components are then assembled into the metallic shell.

Due to the need to minimize impedance mismatches and maintain the high vacuum environment, antennas connect the helix to the input and output connectors. Most of the piece parts are supplied by outside vendors. One exception, the "window," a diaphragm which isolates the vacuum from the outside environment, is machined. These parts are stacked onto a fixture along with brazing rings and brazed together in a furnace. The anode,

collector, and gun sub-assemblies are put together in a similar fashion. Purchased piece parts are essentially stacked and brazed.

Once all the sub-assemblies are combined and brazed together, the tube is "exhausted." A high pressure pump creates a vacuum environment within the tube over a period of several hours under elevated temperatures. Permanent magnets and pole pieces are then secured to the sealed tube. Skilled operators shim and shunt the magnets to optimize each tube's performance. Extensive tests assure specification compliance for each tube. Finally, the product is packaged for the specific application and subjected to application dependent environmental tests. Such tests can include vibration and gravitational shock.

## 4.3 Past Work in Cost Estimation

Much research exists for linking product design to cost through manufacturing. Some works focus on connecting design attributes to resource consumption. Others translate that resource consumption into cost. The former focuses on individual processes. Such studies generally use a mixture of process physics, empirical studies, and expert advice. Northrop published a detailed model for calculating labor time in the manual lay-up of composites [Northrop, 1976]. The model's 65 steps consider everything from cutting the material to putting away tools. [Kalpakjian, 1992] has compiled a series of relationships for machining. One can determine processing time, energy consumption, tool wear, etc. for milling and turning operations.

The second tier in cost modeling relies on industrial economics, manufacturing systems theory, and accounting. [Whitney and Nevins, 1989] present a methodology for calculating assembly cost. One can easily compare manual methods to automated implementations using their devised system. [Allan et. al., 1990] touch upon manufacturing system issues. Idle times and work-in-process inventory are found in addition to labor, tool, and machine costs using queuing theory. [Ong, 1993] utilizes activities based accounting (ABC) to capture unit, batch, and product level costs to support wire harness design.

Each of the works listed above made a tradeoff between accuracy and modeling effort. Using process physics for the first tier and discrete event simulation for the second provides high accuracy, but also demands great effort. Expert advice and simple accounting equations lie at the other end of

the spectrum. The best balance to strike in the tradeoff is situation dependent making cost modeling somewhat of an art.

## 4.4 Cost Estimation at the Manufacturer

In the TWT industry, the balance is driven by time constraints. Estimating the cost of a design must be done within a few days. During this time, the engineer continually searches for inexpensive methods to manufacture each proposed design. The manufacturing process is broken down into process steps. The labor time and material consumed at each step of the process are estimated. As mentioned in Chapter Two, each proposed design is similar to a past one. Therefore, the resource consumption of most steps is based on past data. Manufacturing changes that change or add new tasks are usually estimated by analogy. A single, fixed labor rate is used for all workers. Past experience with vendors is drawn upon to determine the price of each material. Fixed costs considered are engineering time during design and development efforts or the purchase of new equipment. The engineer uses his own experience on past jobs to predict use of the first resource. Quotes from vendors can be obtained to approximate prices for the latter.

Time is simply not available to delve into the physics or available empirical research for all the process changes. For example, the thermal properties of the tube can be improved if the helix, rod, and tube are brazed together. Before such a brazing process can be performed, the ceramic rods need to be metallized. This requires the use of ion sputtering. The physics of ion sputtering are not explored, rather a few tests runs are tried during feasibility studies and the processing time estimated based from that experience.

In addition to time constraints, uncontrollable variations in cost deter the engineer from using more accurate methods. Operator skill plays a large role. Occasionally, workers change jobs, dramatically altering processing times and yields. Such occurrences are hard to predict, causing cost estimations to be thrown off by as much as a factor of two. These variations effectively drown out detailed estimation.

## 4.5 Model Description

After the factory visit, a questionnaire was sent out to the engineer. The questionnaire asked him to list potential changes in the current manufacturing process that would alter the design parameters from their baseline values. Follow-up discussions clarified the data acquired in the survey to yield the connections between design, manufacturing, and cost. Changes that can be made to the manufacturing process are called strategies. Figure 4-1 lists the strategies available in the model along with the design parameters and resource consumptions they affect.

### 4.5.1 Linking Manufacturing to Design

Strategies can change design parameters in either of two ways. Some process changes allow one design parameter to be placed anywhere within a range of values. Changing the mandrel size during the winding operation is such an example. One can order a mandrel size of any diameter from the supplier, thus any helix radius can be reached once the strategy is chosen. The winding machine at the manufacturer is already set up to handle any helix radius that would ever realistically be requested. Similarly, values for the phratio, shratio, vhratio, and helix length can be set to any practical value by adopting the appropriate strategy. The only limiting range is the gun's perveance, ranging from 0.45 to 0.57 micropervs.

Design parameters can also be set to fixed values by strategies. For instance, arranging assembly and brazing centers to create a four stage collector raises collector efficiency to 80%. Often, more than one strategy affects a design parameter. The design parameter's value for each combination of influential strategies must be determined. The estimations provided by the engineer were based on observations collected from research and development efforts. In the example, mathematical simulations of four stage collectors promise an efficiency of 90%. In the past, such simulations usually overestimate efficiency by 10 to 5%. Thus, an efficiency around 80% was chosen to be conservative.

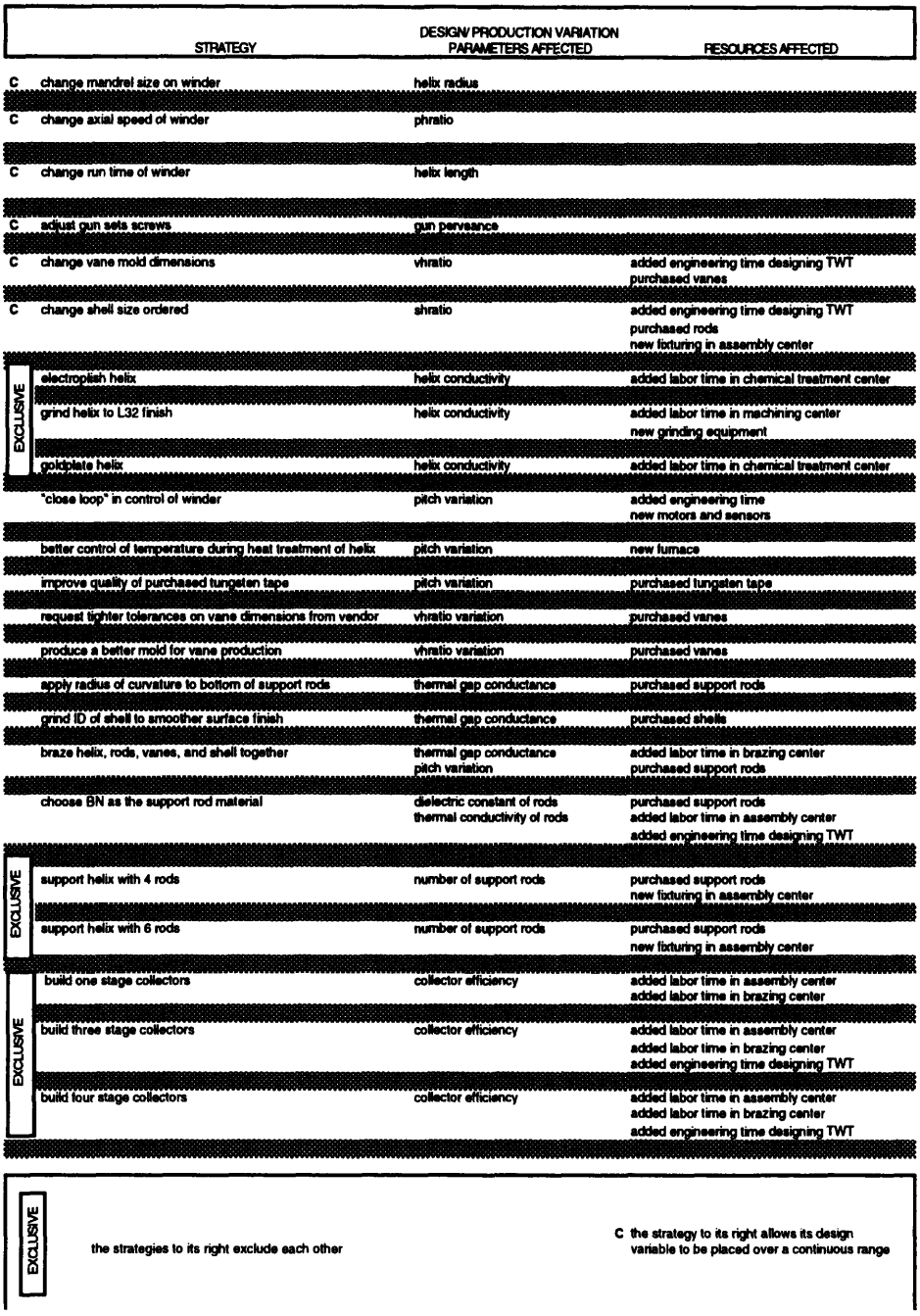


Figure 4-1: The Modeled Manufacturing Strategies and Their Influence

### 4.5.2 Linking Manufacturing to Cost

Instead of attempting to predict cost directly from manufacturing strategies, the link is accomplished through the amount and type of resources consumed. The engineer provided the change in resource consumption for each strategy or combination of strategies and resulting costs. In this manner costs could obtained through the following simple equation:

$$Unit\ Cost = \sum_{i=1}^{n} VRC_i + \left(\frac{1}{PV}\right) \bullet \sum_{j=1}^{n} FRC_j + Current\ Cost \qquad (4\text{-}1)$$

where PV is the production volume of the order , VRC are resource costs changes that are charged to each unit, and FRC are resource costs changes that are charged to the whole production order. Both VRC and FRC are nothing more than the price of the resource times the amount consumed. Explicit accounting for resource changes improves estimation accuracy without overly inflating the estimation effort. As detailed above, the engineer naturally thinks in terms of resources consumed. The approach also allowed the author to check the engineer's estimates. Resource changes not initially considered by the engineer could be proposed based on the author's knowledge of the manufacturing process. For example, changing the number of support rods not only increases the amount of rods purchased but also changes the labor time required to assemble the helix, rods, vane and shell together.

There exist 1,179,648 combinations of strategies. Without some sort of cost structure, all combinations would have to be evaluated. Equation (4-1) already links changes in resource costs to changes in the unit cost of the product. One only needs to link resource costs to manufacturing strategies. Figure 4-1 reveals only a few strategies affect the same resources. Therefore, for each resource, only a few combinations need to be examined to predict how its cost changes over all 1,179,648 combinations.

Types and prices of resources are fairly easy to estimate, consumptions are not. Labor time is a perfect example. Under ideal conditions, it takes approximately 5 minutes of labor time to braze together most sub-assemblies. For a production order of 100 TWT's, the labor time required is much greater, however. Process yields come into play. All brazed products scrapped due to upstream yield problems need to be remade. Sometimes the workers lie idle due to scheduling difficulties. A brazing run actually takes around 1 hour, however, 14 assembly sets are usually processed together. This is not always

the case. During the plant tour, many batches were less than 14, increasing total labor time for the whole order. Resources consumption estimates by the engineer were inflated to compensate for the unmodeled inefficiencies.

By far, the greatest inefficiency at the manufacturer studied was the process yield at the test station. Thus, this factor was directly taken into account modifying equation 4-1 to look as follows:

$$Unit\ Cost = \left(\frac{1}{Test\ Yield}\right)\sum_{i=1}^{n} VRC_i + \left(\frac{1}{PV}\right) \bullet \sum_{j=1}^{n} FRC_j + Current\ Cost \qquad (4\text{-}2)$$

Part tolerances, material quality, etc. are checked during prior steps. However, the performance of the TWT is not checked until this point. Most TWT's that are rejected work, but do not perform within the specifications demanded by their customers. Specifications on small signal gain is a primary example. Each point in a specified frequency range must be greater than a certain value, say 40 dB. In addition, the variation of that gain for all points in the range must not be more than 1 to 3 dB from tube to tube. Essentially a gain envelope is formed. It is not unusual for several tubes in a large batch to lie outside the envelope by 0.5 dB. Only a few of the parts in a reject can be recovered. Most of the sub-assemblies are brazed together. Usually, only the magnets are reusable.

Predicting how the test yield changes as a function of the TWT's design is not easy. All process variations and their impact on all performance measures tested would need to be considered. In the computer tool, only variations in pitch and vhratio and their effect on small signal gain was modeled. The gain envelope is the hardest specification to meet during testing. Variations in helix pitch and vane height have the most influence on this specification. These variations are assumed to have a normal distribution when they arrive at the testing station. The distribution's mean is assumed to lie on the designed value while the variance is allowed to take on values that were estimated by the engineer and dependent on the manufacturing strategies chosen. In the past, the engineer had used Taguchi experiments to determine the three sigma values of the two distributions. Assuming independence between these two variations, the composite variation is merely the multiplication of these two distributions. The independence argument is tough to prove without statistically significant evidence. However, vane height variations can primarily be traced to the shell assembly step, whereas pitch variations are thought to originate from

the processing steps on the helix before assembly and from the thermal expansions during the exhaustion process. Over this distribution of variations entering the testing station, only a certain fraction will allow the tube to be within the performance envelope. The percentage of the composite distribution within this area is the process yield. The exact calculation of this area is costly timewise. The calculation of gain is highly nonlinear, containing many interactions between the design parameters. The gain at each point in the design space is dependent on the level of other design parameters besides phratio and vhratio. Gain would have to be calculated for every design point in the space. To reduce the computational time, the effect of each variation on gain is approximated as linear. Formally, the equation assumed is:

$$Gain = A \bullet phratio\ variation + B \bullet vhratio\ variation \tag{4-4}$$

*if* A and B are defined as:

$$A = \left( \frac{dBGain_{\Delta phratio} - dBGain_0}{\Delta phratio} \right) \tag{4-5}$$

$$B = \left( \frac{dBGain_{\Delta vhratio} - dBGain_0}{\Delta vhratio} \right) \tag{4-6}$$

where $dBGain_0$ is the small signal gain at the current design point, $dBGain_{\Delta phratio}$ and $dBGain_{\Delta vhratio}$ are the gains when the variations $\Delta phratio$ or $\Delta vhratio$ are added to their respective design parameters. $\Delta phratio$ and $\Delta vhratio$ are three times the current standard deviation of the respective parameters upon arriving at the test station. With this linear model, the acceptability area is as shown in Figure 4-2. Vcrit and Pcrit are the critical values at which variations in only one of the parameters pushes gain beyond the envelope. They are calculated from the following relations:

$$Pcrit = \frac{Gain_U - Gain_0}{A} \tag{4-7}$$

$$Vcrit = \frac{Gain_U - Gain_0}{B} \tag{4-8}$$

where $dBGain_U$ is the upper limit on the small signal gain envelope. Since the variations of helix pitch and vane height are independent of one another, the probability density contours are symmetric about the x and y axes of

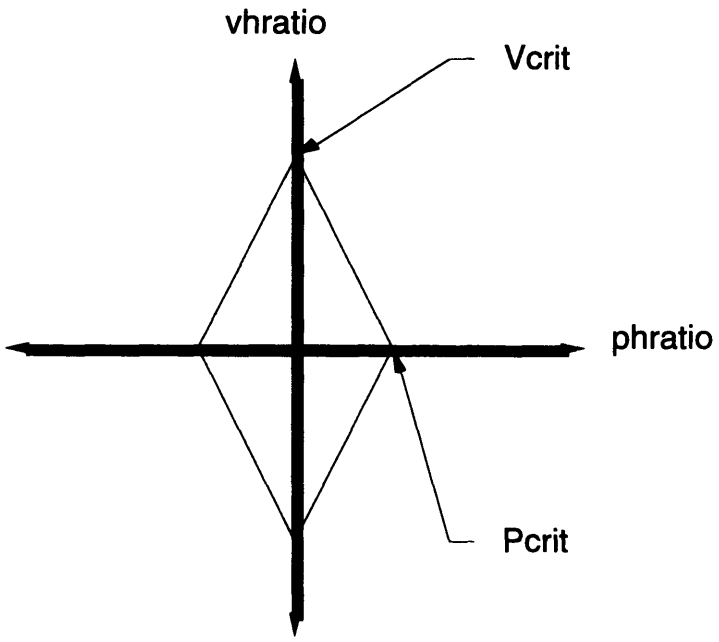


Figure 4-2: Acceptable Area Within the Joint Probability Distribution for vhratio and phratio

Figure 4-2. The problem reduces down to finding the probability over the first quadrant. The basic problem can be stated as:

$$Yield = 4 \bullet \left( P\left\{ \left( \frac{phratio}{Pcrit} \right) + \left( \frac{vhratio}{Vcrit} \right) < 1 \right\} - P\{phratio < 0\} - P\{vhratio < 0\} \right) \tag{4-9}$$

where P{a < b} denotes the probability that the random variable a is less than b. If X is defined as $\left(\frac{phratio}{Pcrit}\right) + \left(\frac{vhratio}{Vcrit}\right)$, X is a normal random variable with mean equal to zero and variance equal to $\left(\frac{Ptol}{Pcrit}\right)^2 + \left(\frac{Vtol}{Vcrit}\right)^2$.

### 4.5.3 Descriptions of the Manufacturing Choices and Their Influence

**Helix Length, Phratio, Radius, and Gun Perveance**

A decision to change any one of these affects only one design parameter. All have no significant impact on cost. The winding machine allows helices to be wound to lengths as high as two and a half feet. Such a length is well beyond the range needed for MPM tubes. Although longer lengths take slightly longer to wind, the effect is negligible. In fact, it takes as long to set up and inspect each sample as it takes to wind it.

As mentioned before, increasing the diameter is merely a matter of winding on a larger mandrel. Although the mandrels are made from machined beryllium, the changes in cost are minimal. The axial and rotational motions of the winding machine can be adjusted through computer input. This allows one to easily alter the phratio. The gun's perveance can be changed through a series of screws. These process flexibilities within the winding operation and gun are not accidents. The manufacturer has specifically designed them to permit changes in product performance for a minimal cost.

**Vane or Shell to Helix Radius Ratios**

As mentioned in the previous chapter, the manufacturer uses computer simulations to aid in the designing of the TWT. The simulations cannot directly model changes in either the vane or shell to helix radius ratio. In addition, past design changes rarely included changing these two parameters. As a result, proposed designs that change these two quantities require significantly more analysis than those designs with more traditional

design changes such altering phratio. Research and development costs rise as result.

**Helix Electrical Conductivity**

Three treatments aim to improve the surface finish of the helix, increasing its electrical conductivity. A chemical bath is used in electropolishing. Ions form currents which etch away at the helix's surface, focusing on the roughest areas. Electropolishing adds an extra process step. The manufacturer already has most of the equipment needed as etching is currently done to remove the helix from the mandrel. Only more labor would be required. The process had been performed in the past at the plant. The added labor time is based on this past experience

Similarly, gold plating employs a chemical process to deposit a fine layer of gold onto the helix. Again, little equipment would need to be purchased. The dominating costs stem from the added labor to perform the step. Since the task is similar in nature to the other chemical bath procedures, the time was based on them.

Another option is to smooth the helix's surface finish through further grinding. A grinding process currently exists which grinds the outer diameter of the helix to assure that it fits correctly into the metal shell. A second run through the grinding process, using a finer abrasive, would reduce the surface roughness. New tools would have to purchased along with more operator time. The engineer drew estimates of the new grinding tool's price and amount of extra labor time from current grinding procedures and equipment.

**Pitch Tolerance**

During the winding of the tungsten tape, axial and rotational speeds are open loop controlled. At the beginning of each day, the winding machine is adjusted to reduce the variation of the helix's pitch. The adjustment process is primarily done to the wire guide that feeds the tape to the revolving mandrel. The variation of the pitch in this process could be significantly improved if closed loop control of the axial and rotational speeds were performed. The engineer mentioned the need for new motors and additional programming. The purchase of the motors and other control equipment as well as the engineering time spent to implement the new controller and alter the current program raise fixed costs.

After winding, the helix is heat treated to remove the stress incurred during winding. The furnace's task is to repeatably produce a time/temperature curve that relieves stress to reduce "spring back," without leaving the tungsten too brittle. Although the optimum curve has been found, the current furnace has difficulty maintaining it. The purchase of a new furnace would improve the situation.

Another improvement strategy focuses on the tungsten material itself. The tape is bought from a supplier. Defects, such as cracks and voids, degrade the repeatability of the pitch during processing. Only one tungsten tape supplier, HCross, exists. The quality could be improved, but would require working with the supplier to localize the quality problems in their manufacturing process. This translates into added engineering time. The engineer suspects HCross will force his company to pay for any specialized tooling required in addition to higher prices per reel. Such estimates of such costs are difficult to make as one cannot know before hand what part of the supplier's process needs to be improved and how that translates into cost. However, past, similar experiences with other sub-components suppliers can be used to get rough estimates.

**Variations in Vane Height**

Changes in the radial dimensions of the loading vanes profoundly affects the gain of the TWT. As a result, further controlling the variation of the vane during manufacturing would lead to higher yields. The vanes are outsourced, but the tooling was made at the manufacturer. Improving the vane tolerance to ±0.2 thousands of an inch could be achieved by simply testing each vane and removing those that do not meet the tolerance. This means lower yield for the vendor and higher material prices for the manufacturer. However, reducing variation down to ±0.1 thousands of an inch would require new tooling. In addition, it would take several weeks of testing and tweaking to stabilize the process with the new mold. Both the production of the new mold as well as the adjustment period translate into added fixed costs. Their values were deduced from experience with the installation of the current mold.

**Thermal contact between rods and shell**

The shape of the supports plays a key role in determining the thermal gap conductivities. Currently, the surface of the rod pressing against the helix has a radius. Radiusing effectively increases the contact area between the rods and the helix. This technique is not being applied to the other end of the rod, where is comes in contact with the shell. Radiusing this other end of the rod would therefore improve the thermal gap conductivity between the rod and shell. The rods are bought from a supplier. Determining the additional cost is therefore difficult as the engineer is not intimately familiar with the process for shaping the rods. Directly contacting suppliers would provide a better estimate than is currently being used. Unfortunately, time constraints did not permit such an investigation.

The thermal gap coefficient could also be improved by reducing the surface roughness over the shell's inner diameter. A honing operation could be setup to polish the inner surface. The manufacture studied does not have machinery to perform this operation, but the suppliers of the tube material do. The same estimation difficulties discussed in radiusing the support rods apply here.

**Pitch Variation and Thermal Conductivity**

Currently, the helix and support rods are held inside the shell by an interference fit. Brazing the parts together would help to control pitch variations as well as to dissipate heat. During exhaustion of the TWT, the rods expand more than the surrounding shell and helix. These relative displacements alter the helix's pitch. Brazing would prevent relative displacements from occurring. Thermal gap conductance across both the helix-support rod and support rod-shell interfaces can be improved. During brazing, the filler metal wets to the surfaces in the interfaces. All the air pockets found using interference fitting disappear. The extra brazing step would be performed in house. The extra cost from the brazing operation can be easily approximated by referencing current brazing operations. Unfortunately, a layer of brazable metal such as titanium needs to be deposited onto the support rods before the entire sub-assembly can be placed into an oven. Although many metalization techniques exist, the company has found that ion sputtering is the most cost effective. The operation would probably be outsourced. Outsourcing would add a material cost. The

amount can be roughly estimated using past experience with ion sputtering, though the work was research oriented.

**Changing rod material**

Boron Nitride, instead of Beryllium Oxide, can be used to make the support rods. Boron Nitride has better thermal conductivity and a higher dielectric constant. The current rod supplier manufacturers rods from both materials. Boron Nitride is cheaper to purchase from the vendor but would be more difficult to process. The material is more pliable than Beryllium Oxide. Operations such as assembling the helix and support rods into the metal shell would be more difficult. Currently, the shell is slightly deformed and the helix and support rods are inserted into position. The shell cannot be grossly deformed or else it will fail to spring back fully to its original form. The shell deforms just enough to allow the support rods and helix to be slid into position. The operation requires that a great deal of force be applied to the helix and rod. Observation of the insertion revealed that the operator has to use his/her own body weight. Use of Boron Nitride would cause the rods to deform and not slide during this process. New techniques such as combinations of pushing and pulling the rods and helix into position would have to be employed. Overall, the assembly difficulties would cancel out any material costs saved.

**Number of support rods**

Increasing the number of support rods increases the number of thermal paths. Heat is more readily dissipated as a result. More rods also means higher loading. Material cost would naturally rise as more components are being purchased. Unfortunately, even with six rods, the increase in order size would not reduce the purchasing price per rod. Also, the task of inserting the rods into the tube would have to be redesigned. As mentioned before, the shell is deformed to allow the rod and helix to be placed into the shell. Specifically, the shell is deformed into a triangular shape. With four or six rods, this deformation shape would not give the clearance needed. New tooling would need to be devised. Therefore, the use of four or six rods would incur additional tooling costs. The estimation was based on the cost of the current fixture.

**Use of collector stages**

From 1 to 4 stages can used in the collector design. The more stages in a collector the higher the efficiency. The base design uses a two stage collector. Designs exist for all collector stages. These designs must be tailored, however, to the rest of the tube's design. Additional engineering time must therefore be spent. This analysis has been done in the past making the estimates of research and development cost fairly accurate. More stages require more piece parts. In addition to the added piece part cost, the labor time during assembly increases. Past produced TWT have used one, two, and three stage collectors. The added/subtracted variable cost for the one and three stage designs were based on this past experience. The four stage design's piece part count can be compared to that of the three stage design and its cost estimated based on this comparison.

## 4.6 Assessment of Model

The modeling structure used in this section is relatively simple. Unit cost is basically built upon the addition of resource costs. A little effort was required to obtain decent yield equations, but overall, efforts described in this chapter pale compared to some of the work done in the sources discussed in Section 4.3. The engineer was heavily relied upon to produce estimates. The manufacturing strategies were discrete in nature. They influenced a broad range of resources and design parameters. Such breadth does not yield easily to mathematical analysis. Strategies were estimated on a case by case basis. The concept of resources merely breaks the problem down into manageable "chunks." Most of the strategies have been studied by the engineer for quite some time. This prior work made expert opinion a very effective and efficient tool. It is highly likely that radically different techniques would have been used had this not been the case.

While the method is fairly successful for the manufacturer studied, such good news may not extend to other TWT makers. In order for the tool to be useful to a systems integrator, all TWT vendors must be incorporated. Differences between manufacturers will be vast. For example, TWT maker A may have just purchased a new oven. TWT maker B may not have the equipment to perform goldplating. Changes in fixed cost will vary from company to company. Other companies might not have done as much prior cost estimation legwork as the manufacturer studied weakening the power of expert opinion.

# Chapter Five

# Search Techniques

## 5.1 Overview

The chapter begins with a description of the specifications to cost tool's interface. The capability of the tool in manual search mode is then demonstrated using a test case. A description of the automated search algorithm of simulated annealing follows. Several test runs using the algorithm are used to show its effectiveness.

## 5.2 User Interface

Figure 5-1 shows the input and output windows of the computer tool. The program runs in the MATLAB4.2 environment. Since the actual code is stored in text files, the program can run on any platform that supports MATLAB4.2. The actual programming and test cases were done on a Macintosh Quadra 950. The STRATEGIES window allows the user to choose combinations of manufacturing strategies. Users can enter the operating conditions, allocated specifications, and the order quantity under the SPECS window. Once the GO button is selected with the mouse, the program transforms these inputs to performance and cost information. The SEARCH button launches the automated search routine with the inputted choices as the initial starting guess. The results can be seen in the OUTPUT window. Intermediate variables are displayed to help guide the user in finding good designs.

The MATLAB4.2 environment was chosen for several reasons. The application was designed to perform mathematical calculations, particularly in linear algebra. Many of its built in mathematical functions were used. ROOTS, a function that calculates the roots of any polynomial, was used to find the solutions to equation 3-54. The program is well suited to house tailor made computational tools, containing a high level, simple, and robust programming language and graphical user interface tool suite.

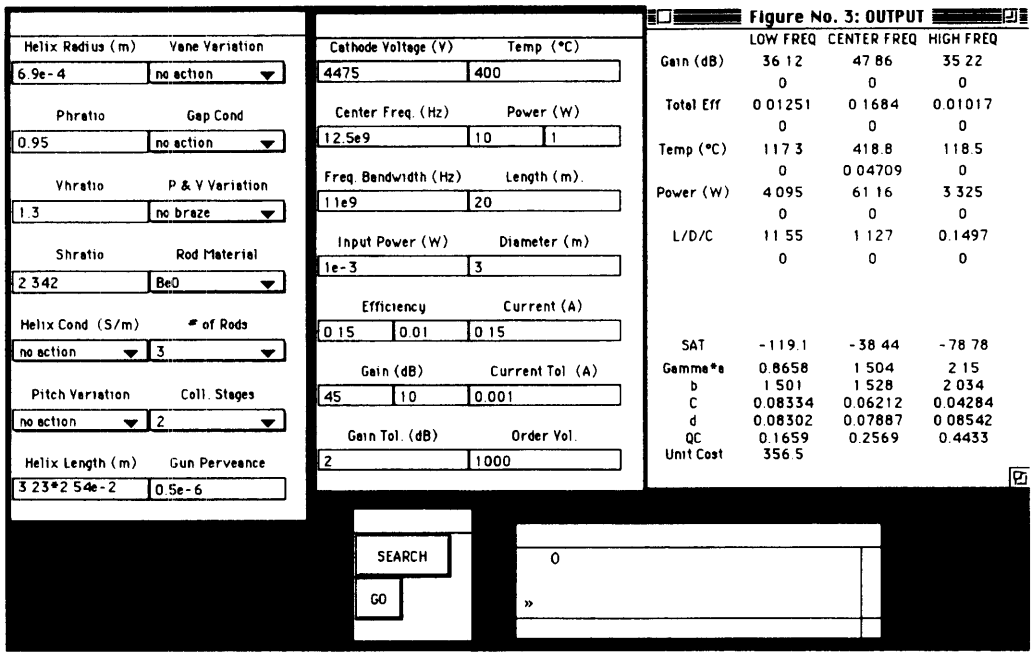


Figure 5-1: Input and Output Interfaces

MATLAB4.2, unfortunately, has one drawback: computational speed. On a Quadra 950, the tool takes just under 10 seconds to evaluate a single set of choices entered by the user. Time studies were run comparing the speed of MATLAB4.2 to traditional programming languages. MATLAB4.2 was found to run an order of magnitude slower. MATLAB4.2 is an interpreter. Such time limitations are not prohibitive during manual searching, but were found to badly hamper automated searching techniques. Ideally, all of the code should be transported over into a general purpose programming language such as C.

The strategy window has a total of seven separate entries. Entries with arrows beside them are discrete in nature. For example, Figure 5-2 shows the choices under the option set marked "Gap Cond." Entries without arrows are editable text boxes. The choices allow one to choose from all of the manufacturing strategies mentioned in Chapter 4.

The specification window is composed of a set of editable text boxes from which all specifications and production volume can be entered. Most of entries are self-explanatory. The entries under one label allow different specifications to be entered for the center and bandwidth edge frequencies. For example, in Figure 5-1, the center frequency gain must be above 60 dB, but the bandwidth edges only need to clear 1 dB.

All boxes in the output window are display only. The leftmost set of boxes label the information displayed to their right. There are three categories: performance variables, intermediate variables, and cost. Gain, Efficiency, Temperature, and Power are displayed for the center, highest, and lowest frequencies in the bandwidth. Performance variables such as Length, Diameter, and DC Beam Current (L/D/C) do not vary with frequency and therefore have only one value.

Under all performance variables is a measure of their ability to satisfy the inputted constraints. For example, the 0 under the Gain parameter at the center frequency indicates that 45 dB is above the gain specification demanded at the center frequency. The 0.04709 under temperature display at the center frequency, however, shows that the helix is hotter than 400 °C at 418.8 °C. These violations increase the farther the performance variable is from its specifications. The values are calculated similar to the way one calculates percent error. The difference between the specification and performance is divided by the specification value. Negative values are reset to zero. The

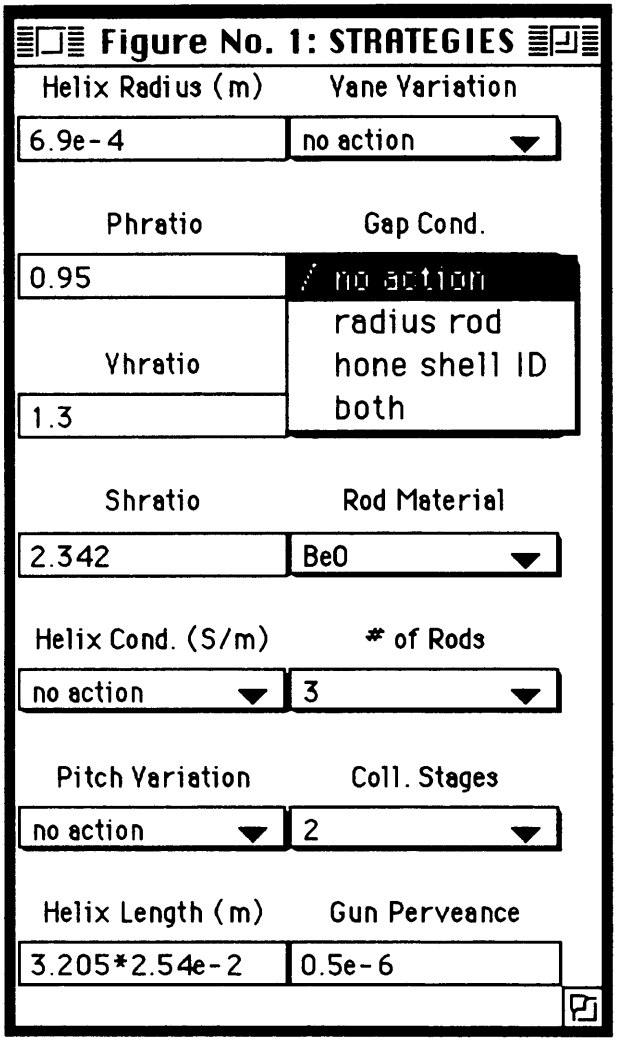


Figure 5-2: Illustration of a Strategy Option Menu with Discrete Choices

percent error method effectively normalizes all the specification violations. A 40 degree violation of a 400°C temperature specification and a 5 dB violation of 50 dB Gain specification are given the same value.

The "SAT" row measures how close the design is to the saturated region. Positive values indicate that the design is in the saturated region. In the saturated region, the TWT performance becomes extremely unstable. Positive values are to be avoided.

The intermediate variables are useful during manual search. For example, Chapter 3 discussed the significance of Pierce's velocity parameter b. It compares the speed of the electron beam to that of the cold circuit velocity wave. For gain to successfully occur, the parameter must be between -2 and 4. In almost all cases, the range is typically even smaller: between 0 and 3. Since variables such as the helix's pitch and the operating voltage influence b, they can be manipulated to maneuver b into the correct range. Focusing on the intermediate variables first allows for the user to choose the better strategies more efficiently.

The cost presented is based upon the method discussed in Chapter 4. The actual value has been multiplied by a constant to protect the proprietary nature of the data.

## 5.3 Manual Search

Figure 5-3 shows the design/process choices and specifications used to begin the manual search test cases. The displayed strategies represent the design the manufacturer will use as a baseline in designing its MPM tubes. No changes from the current manufacturing setup have been implemented. This maintains cost at a low level as most of the strategies focus on improving performance by adding more resources. The resulting design meets all specifications matching actual observation from prototypes. The production volume of 1000 is roughly the anticipated volume for a large order of MPM's. A series of searches can be performed which reveal the tradeoff between increased power in this design and cost. The first set of searches focuses on demanding power while holding all other specifications at their current value. These searches were performed by the author; at each step the thinking process is provided. This detail explains the valuable feedback the tool can give to those trying to understand how specifications affect cost.

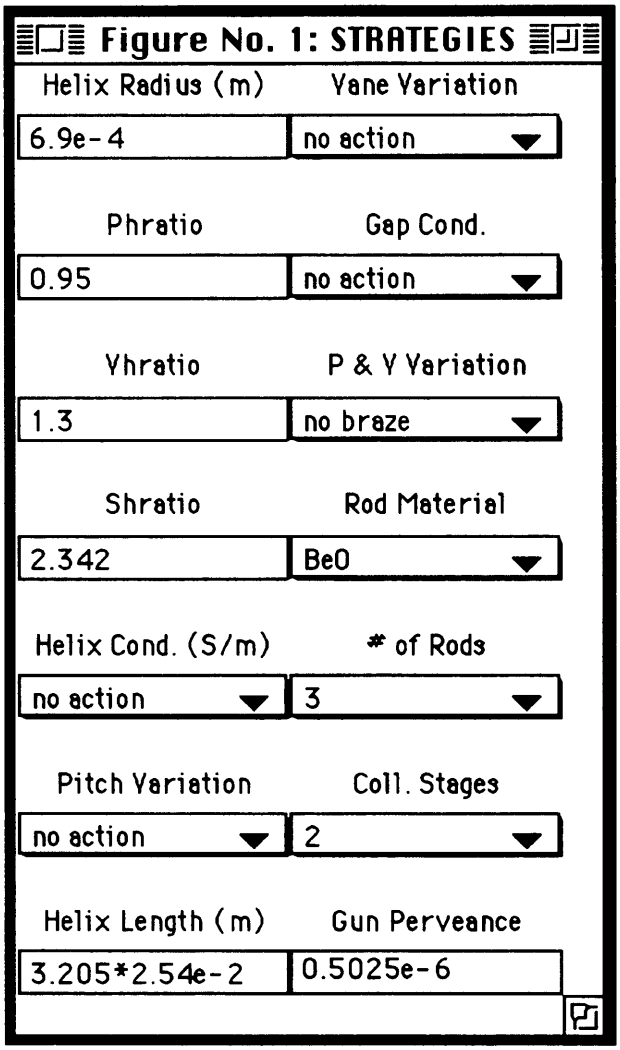


Figure 5-3: Baseline Design Parameters

Since the TWT's length is significantly below its length requirements, it was reasoned that one can always increase power by extending the length of the helix. This extension translates into an increase in gain, efficiency, and power as the beam and the wave have a longer time to interact. Unforetunately, the added power also translates into greater power lost, increasing the temperature on the hottest part of the helix. The current power could be raised to 57.34 Watts by extending the helix's length before the helix temperature uncomfortably neared its 400 °C limits (399 °C). No other specification limits were infringed upon. The helix conductivity, gap conductance, and brazing options were viewed as promising inexpensive ways of improving heat dissipation within the TWT. This would allow one to increase power through further extending the helix's length without breaking the 400 °C barrier. Increasing the number of rods would also help to reduce the heat, but the costs were considered to be higher. Changing the number of rods changes the loading design of the tube. Both the vane to helix radius and shell to helix radius ratios would probably need to be changed forcing extra research and development costs to the tune of at least $50,000. Experimenting with brazing and improving the conductivity yielded several insights. Brazing actually decreased costs. Brazing not only improves heat conductivity, but also reduces pitch variation. The improvement in yield due to the reduced pitch variation outweighed the added resources costs. Note this cost improvement is highly dependent upon the starting baseline design and production volume. Nevertheless, during the search discussed, brazing was automatically chosen due to its ability to both reduce costs and improve the removal of heat ( -11.2 units & -17.5 °C respectively). Brazing allowed the length to be extended to 3.223 inches to yield of power of 60.98 Watts. In addition, all combinations of improving helix pitch tolerance and vane tolerance were examined in an attempt lower costs further. The minimum cost from checking all the combinations was found to be 330.8 by improving the material quality of the tungsten. Therefore, it can be established that for all other specifications held at their current values, tubes with powers from 0 to 60.98 Watts require at most 330.8 units to produce. Lower cost designs may exist. However, we can be fairly confident, based upon the above reasoning about the influences of the various strategies, that we are at the optimum.

Beyond 60.98, the first instinct was to focus on low cost options such as strategies aimed at improving the gap conductance or helix conductivity. Demanding 65 Watts took the cost to 331.9 units as electropolishing was chosen. The target power value of 70 drove the decision to use goldplating as Figure 5-4 indicates. The total cost was 332.7 units. A 75 Watt requirement drove cost up to 335.7 units needing both the shell to be honed and the helix to be goldplated. Both pitch and vane tolerance strategies remained as before.

At this point, careful examination of cost revealed that fixed costs were 30 thousand. The option of changing the number of rods was thereby explored in the hopes of finding cheaper options at the 75 Watt requirement. Changing the number of rods, however, completely alters the loading of the tube requiring all facets of its design to change. Figure 5-5 shows the effect of merely changing the number of rods. By adding the 2 extra rods, we force the wave to travel through more of the dielectric material. This has the effect of slowing the wave down and as is indicated by the increase in b. Gain and thus the power is nearly an inverted parabolic function with respect to b. The first step was to change the pitch to bring it up to its optimum level, at the peak of this parabola. A b equal to 1.005 was found to maximize the small signal gain. Figure 5-6 shows the results Immediately one notices the sharp drop in gain as compared to the prior 3 rod design at the center frequency. This is due to the increases in C from 0.062 to 0.059 and the increases in d and QC ( 0.063 to 0.066 and 0.26 to 0.28 respectively). Therefore, the increase in loading has the effect of increasing loss within the tube and decreasing the interaction efficiency. Fortunately, the length can simply be extended to accommodate. A length of 3.627 inches yields adequate power but forces the total efficiency at the lowest frequency to dip below its 1% value. This was not surprising as changing the loading also changes the dispersion characteristics of the tube. The difference between the velocities of the wave at low compared to center frequency has increased. The evidence is encapsulated in the b parameter. The vane to helix radius ratio could have been adjusted to counteract the effect, but the added development cost was felt to outweigh any gain. Instead, the helix radius was changed. By increasing the helix radius, the peak operation frequency is shifted to lower values. A radius of 7.05e-4 combined with a length of 3.555 brought the tube into meeting all specifications as shown in Figure 5-7. Luckily, the shift in

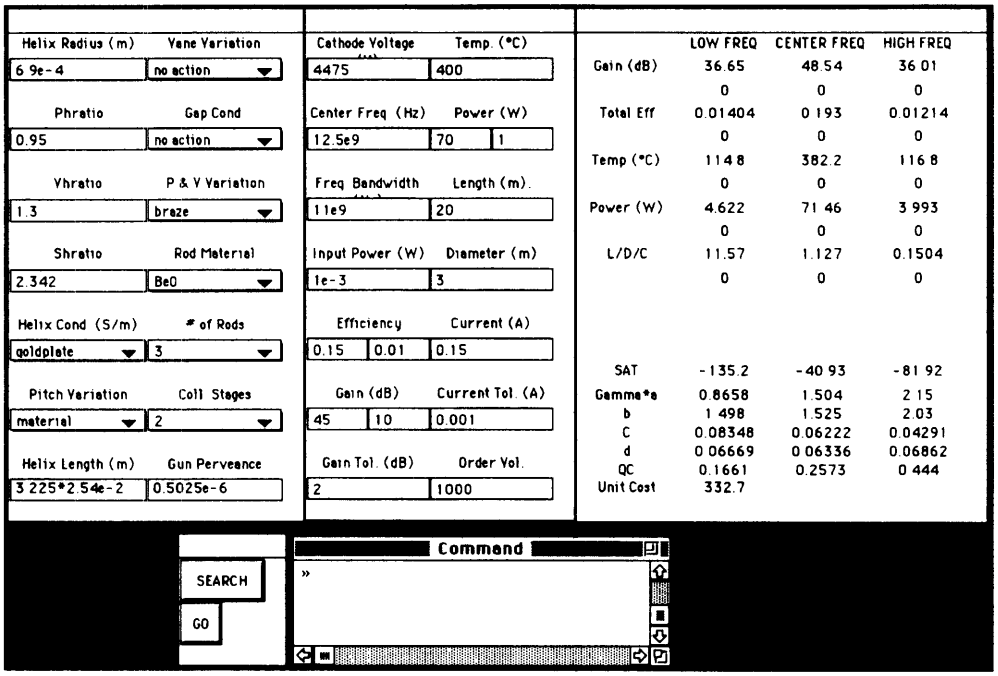


Figure 5-4: TWT Design with 70 Watts of Output Power

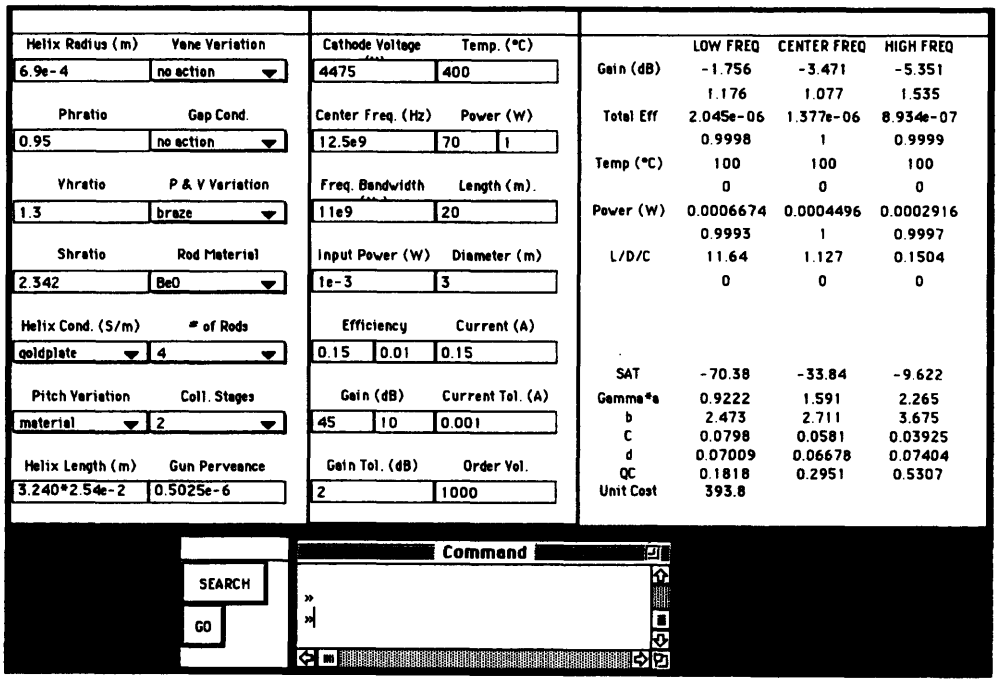


Figure 5-5: Effect of Changing # of Rods

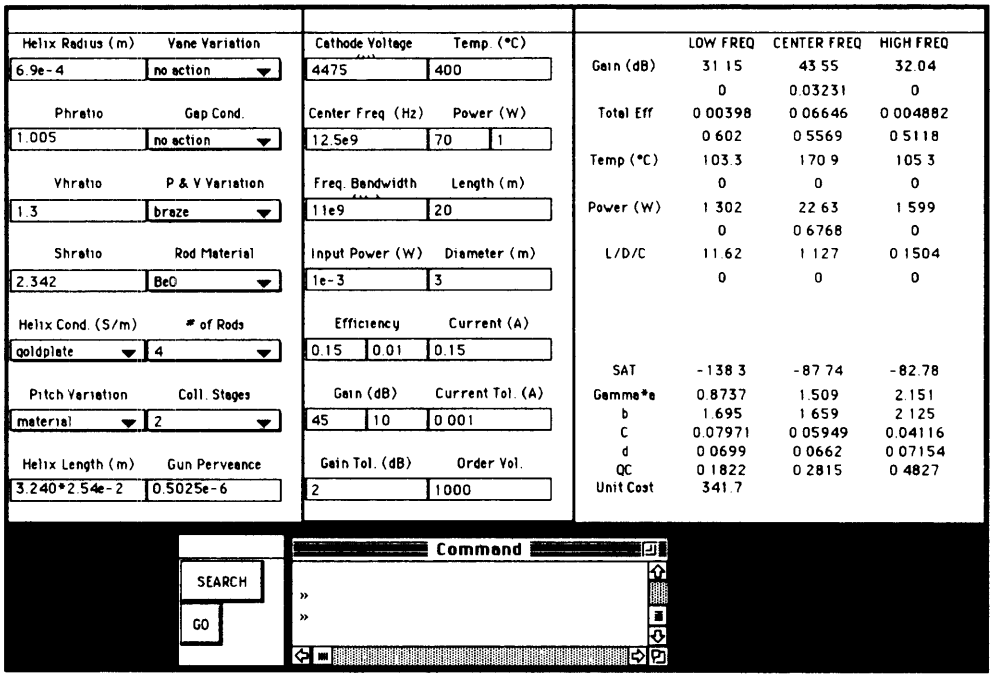


Figure 5-6: Effect of Changing b

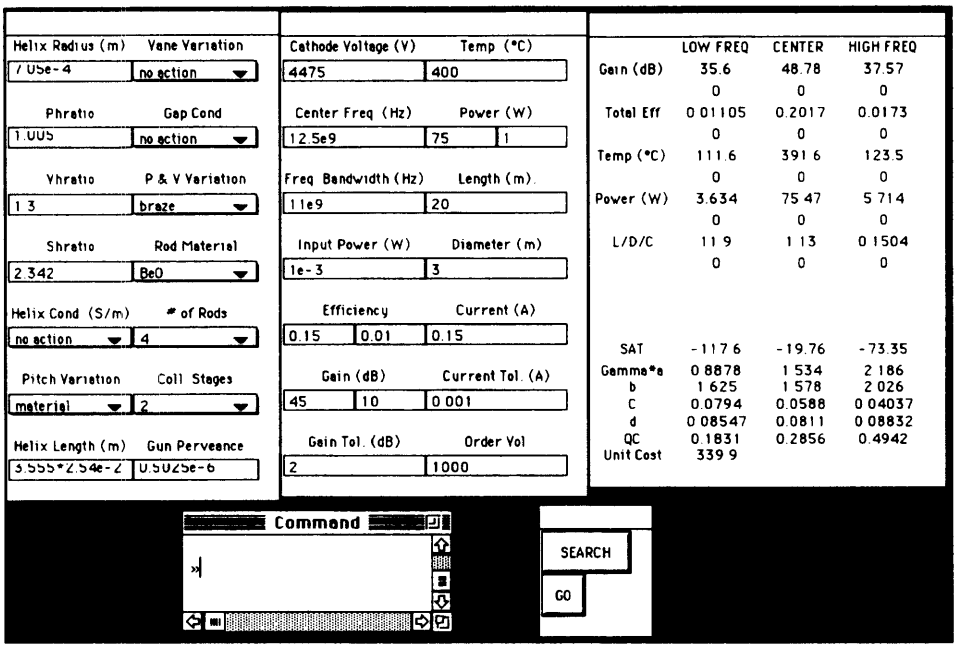


Figure 5-7: 4 Rod Design that Produces 75 Watts

frequency did not excessively reduce the high frequency efficiency below its limit. Searching again through the various options for reducing tolerances yields the combined strategy of demanding tighter tolerances from the supplier of the vanes along with buying extra equipment to improve the precision of the winding machine. The resulting cost of 339.9 units is not low enough to warrant the radical design change.

However, if the limit is increased up to 80 Watts, the design must be used. Using the 3 rod design, 76.2 Watts is the highest one can obtain using the best combinations from the conductivity and gap conductance improvement strategies. The combination of the four rod design with electroplating easily satisfies the constraint at 3.557 inches. The total cost is 341 units with the optimum tolerance reduction strategy of improving the purchased tungsten for the helix.

Adding a double radius to the rod to above set of decisions allows the design barely to reach 85 Watts at a cost of 353 (length equal to 3.5717). The optimum tolerancing falls back to combining new winding equipment with tighter tolerancing of the purchased vanes. Cheapest designs for 90 and 95 Watts use goldplate alone at a cost of 353.7. In order to reach 100 Watts, six rods need to be employed. The redesign is presented in Figure 5-8. Notice, that in this case, the dispersion increase from the two additional rods forced a shell and vane redesign increasing costs dramatically.

Figure 5-9 presents a plot highlighting the tradeoff between power and cost for the particular base design studied. This curve holds true only if all other specifications are held fixed. Changing other specifications in concert with power can yield radically different cost curves. The test case demonstrates the power of performing cost estimation in the optimization framework used by the model. Changes in the product's design and corresponding manufacturing plan underlie every change in cost along the tradeoff curve. The design shifts can range from relatively minor to complete overhauls. Increasing the power in the 60 to 75 Watts range demanded improvements in electrical conductivity and thermal gap conductance. Past 76 Watts, the number of rods, pitch, and helix radius were altered to achieve the desired performance. A complete overhaul of the loading configuration along with the above changes boosted the power capability up to 100 Watts. Changing the vane to helix and shell to helix radius ratios sunk large amounts of costs. As Figure 5-9 displays, the tradeoff curve increased sharply

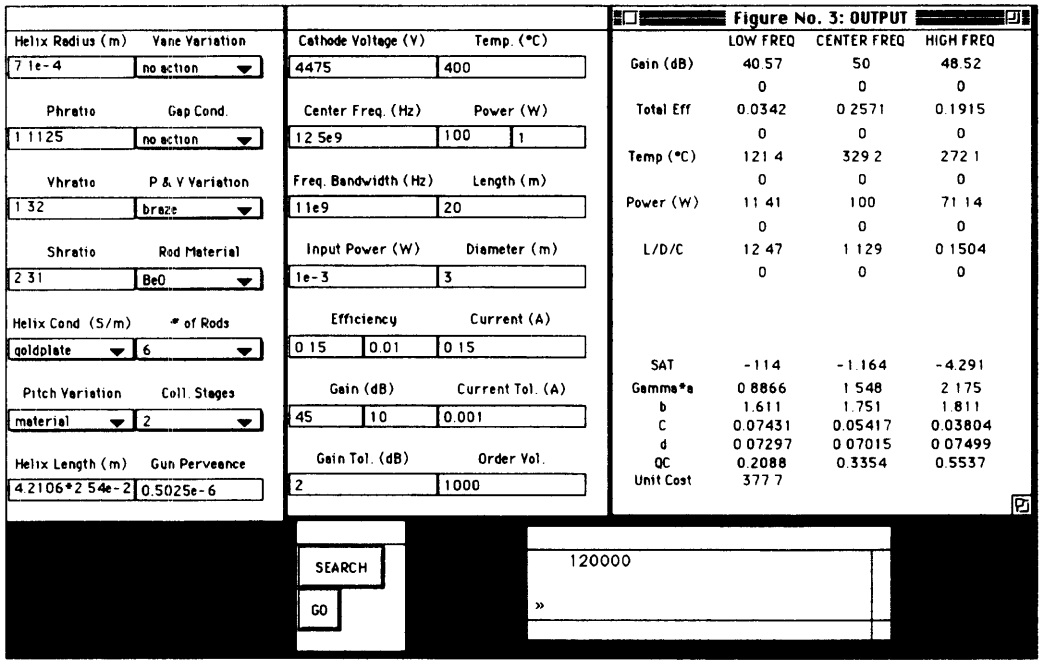


Figure 5-8: 6 Rod Design that Produces 100 Watts

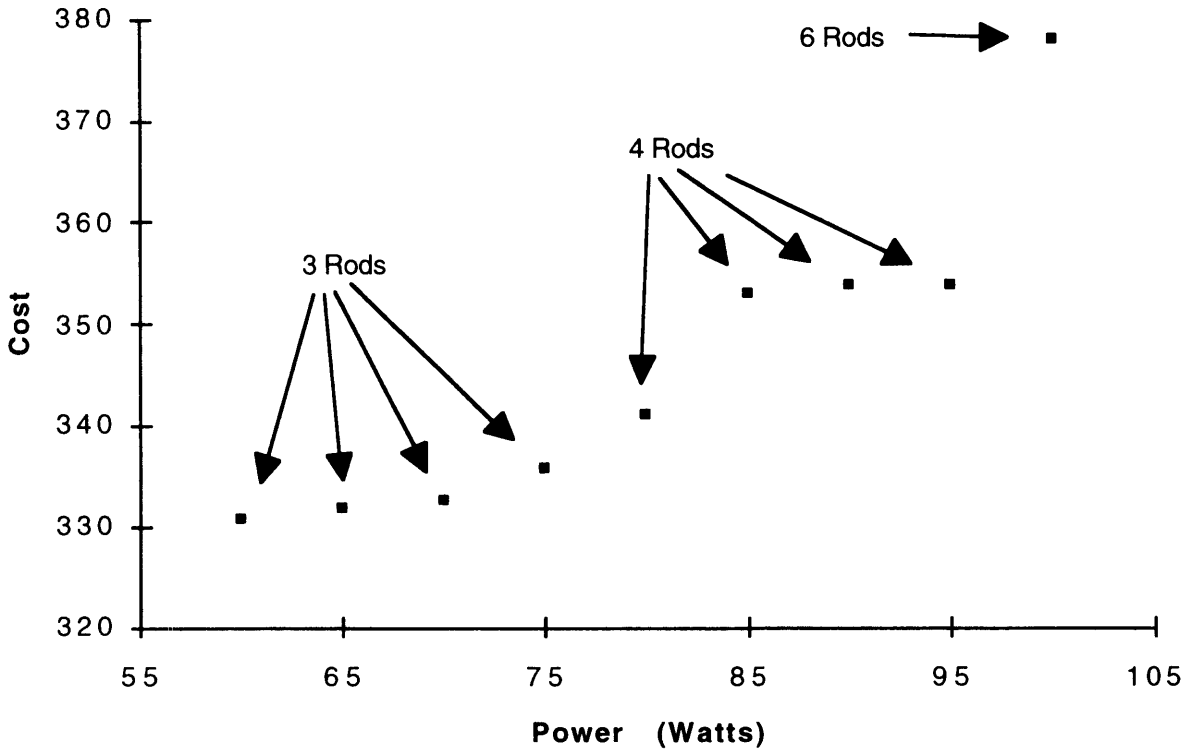


Figure 5-9: Power vs. Cost Curve

at 100 Watts. Such information allows one to locate and understand areas in which a huge price must be paid for small gains in performance.

## 5.4 Automatic Search

Unforetunately, manual searching cannot always be used effectively by the systems designers to derive tradeoff curves. There is no way to be completely confident that the tradeoff curve in Figures 5-9 displays the lowest possible cost. The above discussion, explaining the thinking behind the search, only suggests that the designs chosen to create the curves were close in cost to their respective optimum solutions. In the derived tradeoff curve, only specification was varied. During real use of the tool, the systems integrator may want to vary several specifications at once. Worse, the search was conducted by the model's creator, someone with a highly detailed understanding of the relations the model incorporates. As is evident from the above explanations, this knowledge was used to efficiently guide the search. Systems integrators have significantly less prior knowledge making their search less effective. Such difficulties point toward the need to provide automatic methods for finding good solutions.

The optimization problem faced is extremely difficult. The problem is large. There exist 14 separate option categories. Combining the 8 discrete choices yields 147,456 options. The 6 continuous parameters offer an infinite number of possibilities. The problem cannot proven to be convex. Most of the analytical equations used are nonlinear. Fortunately, prior work has been done on problems of such difficulty ([Aarts, 1989], [Milner, 1991], and [Ramaswmay, 1993]). Search techniques such as genetic algorithms and simulated annealing can usually yield surprisingly good solutions. It is essential to point out that no general purpose methodology exists that can guarantee finding the location of the best solution. The algorithms can only promise that a high probability exists that the proposed solutions lie within a small top percentage.

[Milner, 1991] uses simulated annealing to solve a large scale, discrete, and nonlinear problem in assembly. The search technique and many of his findings on how to setup the algorithm were used to build an automatic search function. Figure 5-10 shows the basic structure of the algorithm in pseudo-code. The technique originated from research in condensed matter physics on the process of annealing. During the annealing process, a solid is

```
Get an initial solution x
Get an initial temperature T
While ( not yet frozen) do
        For ( i = 1 to n ) do
                Set y = random neighbor of x
                Set D = f(y) - f(x)
                If ( D ≤ 0)
                        Set x = y
                        Set counter = 0
                Else
                        Set x = y with probability e^-D/T
        Set T=Tempfactor * T
        If (Accepted Percent of N trials < minpercent)
                Set counter = counter +1
        If(counter = 5)
                Set frozen = TRUE
```

Figure 5-10: The Simulated Annealing Algorithm [Milner, 1991]

placed in a heat bath. The temperature of the heat bath starts at the maximum value at which the solid melts. Slowly, the temperature of the heat bath is lowered until the particles arrange themselves into the minimum energy state of the solid. The substance can thought of as a system of particles. A given state of the system is denoted by the position of all particles. As long as thermal equilibrium is reached before each temperature decrement, a stable probability distribution exists over all the possible states.

Combinatorial optimization problems can be solved by drawing an analogy between the particle system and themselves. In the particular problem understudy, each possible solution represents a state. Instead of energy, the unit cost is minimized. The algorithm in Figure 5-10 effectively simulates the reaching of thermal equilibrium and the gradual decreases in temperature. Starting from an initial set of choices, the program randomly generates a choice set and compares it to the current state. If the cost of the proposed solution is less than the current state, it becomes the current state. On the other hand, if the proposed solution is greater, there exists a probability that it will become the current state:

$$P\{accepted\} = e^{-\left(\frac{f(proposed\ state) - f(current\ state)}{T}\right)} \qquad (5\text{-}1)$$

where P{accepted} is the probability that the proposed set of choices is accepted, f(current state) and f(current state) are the costs including penalties at the current and proposed state respectively, and T is the effective "temperature." A series of n iterations are performed at constant T. If the iterations are sufficiently long, an approximately stable probability distribution will exist over all state possibilities. At the end of each set of iterations, T is decreased. The higher the temperature, the more likely the state jumps to a point of higher energy (cost) at the end of these iterations. As the temperature approaches zero, the algorithm is equivalent to local search techniques. The high temperatures in the beginning of the process aid the algorithm in avoiding relatively costly local minima.

Two functions in the algorithm are problem specific: choosing a random neighbor and evaluating the cost of each proposed solution. The chosen neighbor should be, qualitatively, a small departure from the current option. Alternatively, the changes should provide enough freedom to insure that all possible options can be reached by a finite series of moves from the current state. The program effectively alters one parameter out of the existing

14 by one level. Continuous variables are broken down into a set of discrete choices. From discussions with the engineer, ranges were assigned to each continuous choice. One percent of the baseline value was used as the distance between each of the discrete points. For example, pitch to helix radius ratio could range from 0 to 2. The baseline value for the pitch was rounded to 1. This created a set of values that can be mathematically described as:

$$phratio = \{0, 0.01, 0.02, \ldots, 1.99, 2.00\} \quad (5\text{-}2)$$

The 1% value was based on empirical experimentation with the various parameters. Overall, 1% changes in the continuos parameters yielded small changes in performance. Too small of a value would dramatically decrease the ability of the algorithm to explore values over the entire range of the variable. Too large a value might exclude low cost options in between levels. No case is made for 1% being the best value, only a reasonable one.

Evaluating the cost function is more than determining its unit cost. Simulated annealing does not directly recognize constraints. Instead, they are indirectly considered using a penalty function. If a constraint is violated, the effective cost is increased. The violations mentioned in Section 2 were entered into the following formula, assigning a penalty to add to the unit manufacturing cost:

$$Penalty = P \bullet (Violation\ for\ Gain + Violation\ for\ Temp + \ldots + Violation\ for\ SAT) \quad (5\text{-}3)$$

where P is a weighting factor. Most penalty functions in optimization literature grow nonlinearly with increasing violation levels. A linear function was chosen provide the algorithm the capability to traverse far outside of the constrained set of choices. This allowed quick moves from one workable configuration to another. For example, in the manual searching, altering the number of rods caused many constraint violations. However, subsequent changes in pitch, helix radius, length, etc. brought the design back into feasible space where a lower cost design resided. Since a move changes one parameter at a time, points with high violation values must be tolerated to reach the better designs. Empirically, most violations range from 0 to 1 or 2. P was set to 1000. The value allowed the algorithm to search through costly designs early in the cooling schedule yet home in on violation free designs toward the end of the cooling schedule.

Careful examination of Figure 5-10 will reveal that there are 4 unspecified parameters: T0, n, tempfactor, minpercent. A great deal of Milner's thesis involves determining the optimum setting for these

parameters through the use of experimentation and theory. Tempfactor and minpercent were set to 0.9 and 0.1 respectively, both values used by Milner. He also notes that T0 should be such that solutions greater than the current point have initially a 0.4 probability of being accepted. Since the acceptance probability for any one of these higher cost points is described by equation 5-1, T0 can be deduced by the following equation:

$$T0 = \frac{-stdev(\ f(proposed\ state) - f(current\ state)\ )}{\ln(0.4)} \qquad (5\text{-}4)$$

where stdev(x) is the observed standard deviation. Empirically, stdev(f(proposed state) - f(current state)) was found to be around 100 meaning that the optimum value for T0 was 415. Finally n should be set to assure that a stable distribution can eventually occur over a the range of choices. Milner suggests that n be set to the size of the neighborhood surrounding each point. Since the function which chooses neighbors to evaluate moves one design parameter at a time, there exists a total of 26 neighbors in most situations. Some design points, like the one shown in Figure 5-8, have less than this number because the algorithm can only move "down" to grinding in the helix electrical conductivity option. For these reasons, n was set at 25.

To test the effectiveness of the automatic search capability, the 100 Watt test case above was used. The tests were conducted on a Silicon Graphics Indy. Each iteration took approximately 2 seconds to complete. The tests can be separated into batches. The first batch examined the variability in the best scores found. The second adjusted the temperature factor to estimate the value of longer search times. Finally, the third set of runs tried a combination of manual search and simulated annealing, hoping the joining of man and machine would yield the best results.

The first series of ten tests had the same baseline design as the manual search case (see Figure 5-3). Figures 5-11 and 5-12 show runs #3 and #7 respectively. The points plotted are the design points reached before each temperature decrement. Therefore, every twenty-fifth point is plotted. Table 1 shows the key information of each run. The frozen score is the value that the algorithm converges to at the end of each run. The best score is the lowest score that was found during the entire search. The best score found varied greatly. The algorithm was generally unable to find a design better than the one found using manual search. Run #7 is the sole exception. Figure 5-14 shows Run #7's best design

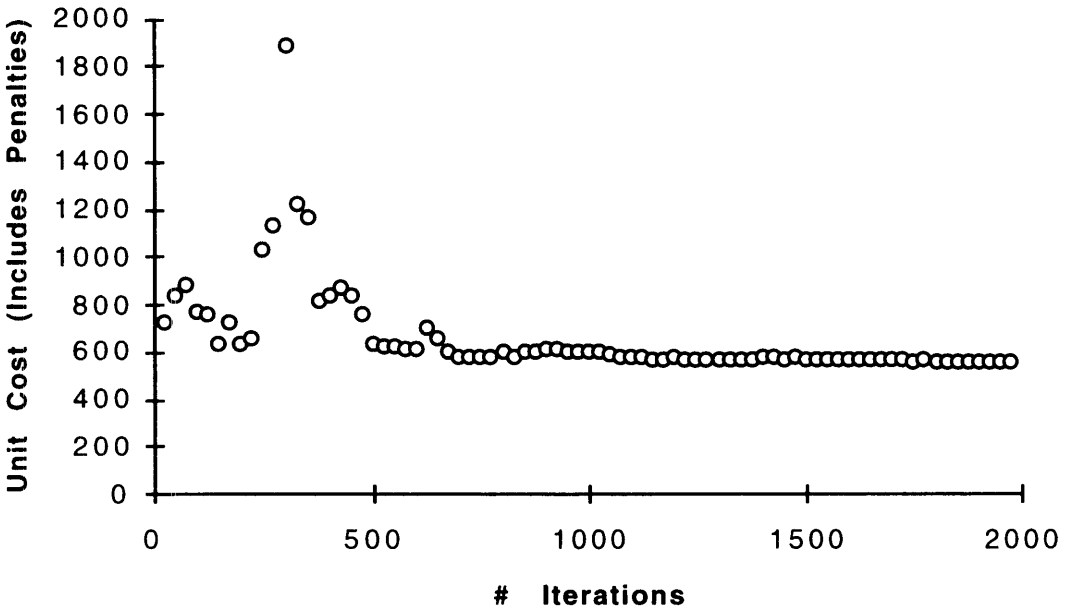


Figure 5-11: A Time History of the Scores Reached During the Third Run of the Simulated Annealing Algorithm

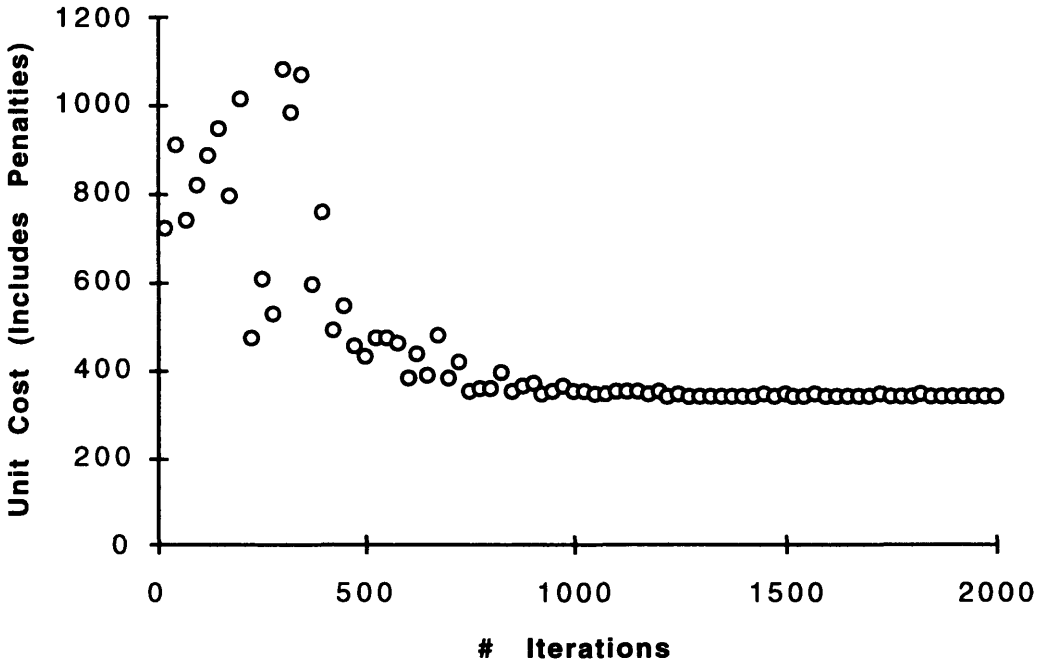


Figure 5-12: A Time History of the Scores Reached During the Seventh Run of the Simulated Annealing Algorithm

| Batch | Run | Iteration Limit | Tempfactor | Rod # and Material | Total # of Iterations | Frozen Score | Best Score |
|---|---|---|---|---|---|---|---|
| 1 | 1 | none | 0.9 | not fixed | 2100 | 588 | 588 |
| 1 | 2 | none | 0.9 | not fixed | 2125 | 597 | 597 |
| 1 | 3 | none | 0.9 | not fixed | 1975 | 559 | 559 |
| 1 | 4 | none | 0.9 | not fixed | 2100 | 600 | 600 |
| 1 | 5 | none | 0.9 | not fixed | 1800 | 564 | 564 |
| 1 | 6 | none | 0.9 | not fixed | 1875 | 571 | 571 |
| 1 | 7 | none | 0.9 | not fixed | 2400 | 341 | 339 |
| 1 | 8 | none | 0.9 | not fixed | 2125 | 581 | 581 |
| 1 | 9 | none | 0.9 | not fixed | 2525 | 595 | 595 |
| 1 | 10 | none | 0.9 | not fixed | 2350 | 591 | 591 |
| | | | | | | | |
| 2 | 1 | 5000 | 0.95 | not fixed | 4100 | 361 | 359 |
| 2 | 2 | 5000 | 0.95 | not fixed | 4225 | 605 | 605 |
| 2 | 3 | 5000 | 0.95 | not fixed | 4500 | 591 | 591 |
| 2 | 4 | 5000 | 0.95 | not fixed | 4250 | 534 | 534 |
| 2 | 5 | 5000 | 0.95 | not fixed | 4050 | 555 | 555 |
| 2 | 6 | 5000 | 0.95 | not fixed | 3850 | 547 | 547 |
| 2 | 7 | 5000 | 0.95 | not fixed | 4100 | 575 | 506 |
| 2 | 8 | 5000 | 0.95 | not fixed | 4000 | 416 | 402 |
| 2 | 9 | 5000 | 0.95 | not fixed | 4125 | 578 | 366 |
| 2 | 10 | 5000 | 0.95 | not fixed | 3875 | 360 | 360 |
| | | | | | | | |
| 3 | 1 | 2000 | 0.9 | fixed | 2000 | 351 | 351 |
| 3 | 2 | 2000 | 0.9 | fixed | 2000 | 379 | 379 |
| 3 | 3 | 2000 | 0.9 | fixed | 2000 | 351 | 351 |
| 3 | 4 | 2000 | 0.9 | fixed | 2000 | 344 | 338 |
| 3 | 5 | 2000 | 0.9 | fixed | 2000 | 380 | 365 |
| 3 | 6 | 2000 | 0.9 | fixed | 2000 | 351 | 351 |
| 3 | 7 | 2000 | 0.9 | fixed | 2000 | 344 | 338 |
| 3 | 8 | 2000 | 0.9 | fixed | 2000 | 380 | 365 |
| 3 | 9 | 2000 | 0.9 | fixed | 2000 | 357 | 357 |
| 3 | 10 | 2000 | 0.9 | fixed | 2000 | 408 | 350 |

Table 4-1: Key Information Produced by Each Test Run

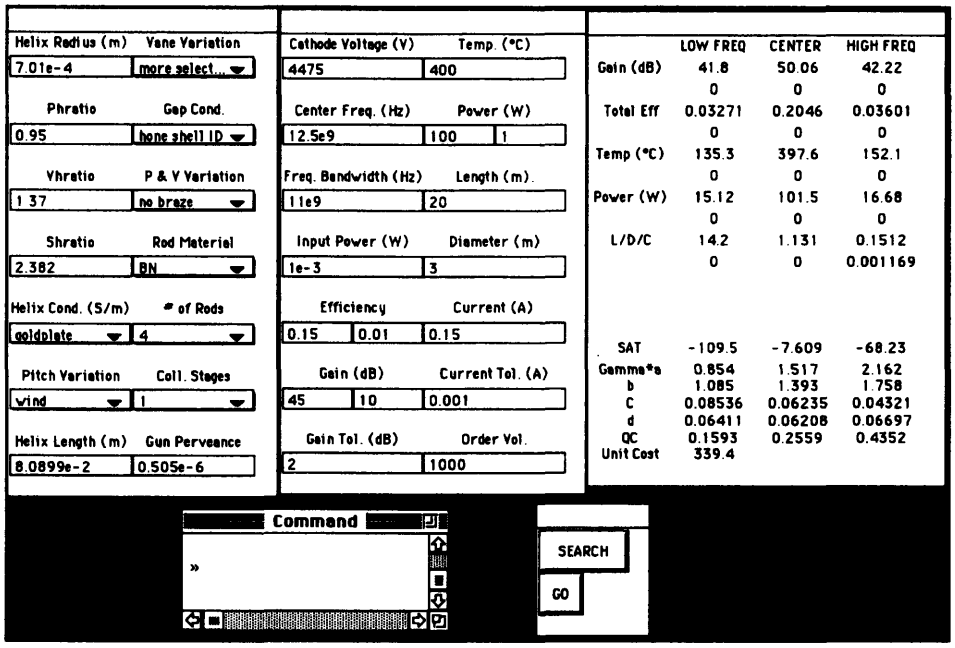


Figure 5-13: Best Design Found by the Seventh Running of the Simulated Annealing Algorithm

(in fact, the best one found in all of the ten runs). The design slightly violates the current specifications. However, increasing the length to 8.11e-2 meters and decreasing the gun's perveance to 5.02e-7 solves the problem with no additional cost. Figure 5-14 shows Run #3's best. 3 rods are used instead of 4 or 6. This choice of 3 rods was evident in all of the best designs (except for Run #7 which chose 4 rods). Since the search routine moves one design parameter at a time, it is forced to move through a series of costly designs to find acceptable designs with more than 3 rods. The runs "cooled" too quickly to allow a strong probability of climbing over the "barriers" in the design space. Most searches were essentially unable to "jump" over the costly barrier that separated 3 rod designs from good 4 or 6 rods designs. Trapped in a local minimum, these searches were doomed to generate infeasible designs. This explains their inability to lower cost past 500 as their designs were penalized quite heavily for the specification violations. Figure 5-14 shows such constraint violations.

One method for increasing the algorithm's ability to escape local minima is to raise the tempfactor. The cooling schedule becomes more gradual and the time to finish a run longer. A batch of ten tests were run at a tempfactor at 0.95. The number iterations was limited to 5000 (200 temperature decrements). Table 1 also shows these tests. Three good designs were found. Although many more tests would need to be run to establish statistical significance, the results nonetheless suggest that the chances of finding a good design increase.

Another way of improving the quality of the searches is to use a combination of manual and automatic searching. A variation of the algorithm was compiled to allow the user to hold certain choices constant. Table 1 reveals the best design found used a rod number and material of 6 and Boron Nitride respectively. Both of these parameters lie far outside the local minimum that traps the initial design. In a series of ten runs, the rod's number and material were fixed to these optimum values throughout the entire search. In these runs, the number of iterations was limited to 2000 (80 temperature decrements). Table 1 shows the results. Each time, the algorithm found good, feasible designs.

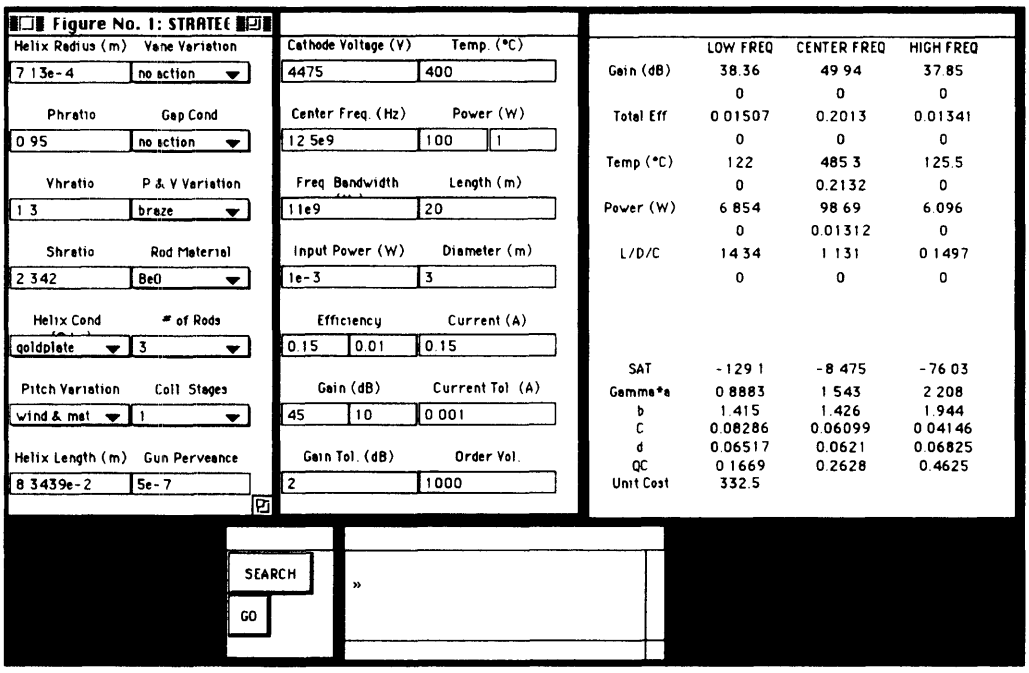


Figure 5-14: Best Design Found by the Third Running of the Simulated Annealing Algorithm

## 5.5 Assessment of Search Techniques

The process of connecting specifications to cost is slow. The combination of manual and automatic search methods identified good points the quickest. Nevertheless, the time scale is still in hours (5 hours for five runs on a Silicon Graphics Indy). Industrial upgrading of the model would increase the time requirements even further. However, much room for improvement exists. The code can be converted over into C. The work in this thesis makes no claim of optimizing the parameter settings in the simulated annealing algorithm. Such "tweaking" would also yield better performance. With effort, one search stands a good chance of taking only minutes. The evidence provided in this thesis is by no means conclusive. A solid statistical analysis of success rates are needed. The current work does demonstrate potential. That, in itself, is an accomplishment.

# Chapter Six

# Conclusion

I constructed a computer tool that can predict the cost of a product called the Traveling Wave Tube (TWT) based upon its specifications. Those that use the TWT to construct MPMs could use a full scale version to quickly understand how specifications drive cost. The program functions as a prototype, exploring the use of optimization and mathematical equations to make the connection between cost and performance demanded. Because the physics of the TWT and the resources used in its manufacture are explicitly modeled, the tool can make relatively detailed cost estimates.

Comparing the model to a simpler one being built by my group at C. S. Draper Laboratory highlights some of its strengths and weaknesses. The simple model is based upon surveying several experts from the TWT industry. They were asked to place a cost value on several specifications combinations. The tool interpolates between these points to construct a multi-dimensional surface that can also calculate cost based upon performance specifications.

Turning the problem into one of optimization more directly captures how TWT designers estimate cost. Every time a cost needs to be estimated, the computer program is free to search among millions of possibilities. As shown in Figure 5-9, specification vs. cost tradeoff curves are not simple, smooth functions. Small changes in specifications sometimes force one to completely change how the TWT is made. Chapter Five's account of increasing the power specification from 95 to 100 Watts illustrates this phenomenon. At the same time, the searching is time consuming. It takes a half a day to confirm a cost estimate for just one design point. Getting an entire curve that compares cost to performance could take a week. The amount of calculations in a full scale implementation may be an order a magnitude more than is currently performed in the prototype. The whole point of building a computer tool was to reduce the time needed to perform the estimations. Converting all of the program's code into C plus tweaking and optimizing the automatic search algorithm should reduce the time to a day. This makes the tool still useful but waters down its effectiveness.

Tradeoff curves using the interpolation method can be built in a matter of minutes. The goal of the systems integrator is to find the specification combination for each of the three sub-components that minimizes the total cost of the MPM. The computer tool developed by the whole group allows more specifications combinations to be examined than the one described here, but estimates each one less accurately. While the simple tool will probably find lower cost MPM designs, inaccuracies in their estimation are more likely to render the results meaningless.

The model in this thesis uses a framework which breaks the problem down into a network of mathematical functions. Breaking the problem down into its essential pieces often makes the model easier to update in the future. For example, changing the shell size adds significant costs as fixturing needs to be replaced. In the future, a flexible fixturing tool may be developed. The price of such a fixturing change (a constant in the computer tool) need only be altered to prevent the model from becoming obsolete. Using the survey method, one must conduct a new survey. In some situations, however, the imposed modularity can have the opposite effect. If the manufacturer studied decides to radically change its baseline design (taper the helix), it may take longer to reconstruct the affected modules than to send out and receive back a new survey.

The road between performance and cost is long and complicated. Everything from the TWT's thermal properties to a supplier's pricing policies must be considered. Most of the modeling is not directly based upon the "physical" laws of the natural sciences or economics. At the same time it is not merely statistical in nature (like the interpolation approach adopted by the group). I have not derived everything from "first principles" nor have I compiled loads of empirical data to establish the trends. Instead, I took an approach somewhere in between. Finding simple, gross relationships that accurately capture the observed trends is a tricky business. With further investigation, however, I am willing the gamble that the prototype can be made to make good predictions. Both economics and business use levels of abstraction to make analysis manageable yet useful. Like performance vs. cost, a natural tradeoff occurs in modeling. Model every detail and the effort required mushrooms; treat the whole system as a "black box" and one produces zero insight into the underlying mechanisms at work. My computer tool was an attempt to achieve a happy medium in the tradeoff

between effort/cost and accuracy/insight. In way, what I tried to do was similar to what the MPM integrators will do each time they have to design an MPM: strike a balance.

# Bibliography


[Aarts,1989] Emile Aarts and Jan Korst. *Simulated Annealing and Boltzman Machines: a stochastic approach to combinatorial optimization and nueral computing.* Wiley, New York, 1989.

[Allan et. al., 1990] David C. Allan and et al. An Engineering Model for Predicting Manufacturing Costs of Aerospace Components. In *Issues in Design/Manufacture Integration*. The American Society of Mechanical Engineers, 1990.

[Arnett et. al., 1973] Henry D. Arnett, Sidney T. Smith, and Lester M. Winslow. *Design Concepts for Dual-Mode Traveling Wave Tubes.* Naval Research Laboratory Memorandum Report 2599, 1973.

[Fanton, 1985] Jeff Fanton. *The "SARA" Large-Signal Program.* Naval Research Laboratory, 1985.

[Gilmour, 1979] Alexander S. Gilmour, Marlin R. Gillette, and Jenn-Tsung Chen. Theoretical and Experimental TWT Helix Loss Determination. *IEEE Transactions on Electron Devices*, Vol. ED-26, No. 10, 1979.

[Gilmour, 1994] Alexander S. Gilmour. *Principles of Traveling Wave Tubes.* Artech House, Boston, 1994.

[Kalpakjian, 1992] Serope Kalpakjian. *Manufacturing Engineering and Technology.* Addison-Wesley, Reading MA, 1992.

[Kravckenko, 1976] N. P. Kravchenko, L. N. Loshakov, Yu N. Pcel'nikov. Evaluation of Three Techniques of Controlling Phase Velocity Dispersion in Helix TWT. in *Proc. Int. Conf. Microwave Tubes in Systems: Problems and Prospects*, 1984.

[Kumar et. al., 1989] Lalit Kumar and et al. Modeling of a Vane-Loaded Helical Slow-Wave Structure for Broad-Band Traveling-Wave Tubes. *IEEE Transactions on Electron Devices*, Vol. 36, No. 9, 1989.

[Milner, 1991] Joseph M. Milner. *The Assembly Sequence Selection Problem: An Application of Simulated Annealing*. Master's thesis, Massachusetts Institute of Technology, 1991.

[Northrop, 1976] Northrop Corporation. *Advanced Composites Cost Estimating Manual (ACCEM)*. AFFDL-TR-76-87, 1976.

[Ong, 1993] N. S. Ong. Activity-based Cost Tables to Support Wire Harness Design. *International Journal of Production Economics*, 29, 1993.

[Palmer, 1992] Raymond W. Palmer. *User's Guide for a Large-Signal Computer Model of the Helical Traveling Wave Tube.* NASA Technical Paper 3251, 1992.

[Pierce, 1950] J. R. Pierce. *Traveling Wave Tubes*. D. Van Nostrand, New York, 1950.

[Ramaswamy, 1993] Rajan Ramaswamy. *Computer Tools for Preliminary Parametric Design.* PhD thesis, Massachusetts Institute of Technology, 1991.

[Rowe, 1965] Joseph E. Rowe. *Nonlinear Electron-Wave Interaction Phenomena.* Academic Press, New York, 1965.

[Sauseng, 1978] O. Sauseng. Thermal Properties and Power Capabilities of Helix Structures for Millimeter Waves. *Technical Digest*, IEEE, 1978.

[Srivastava and Joshi, 1993] Vishnu Srivastava and S. N. Joshi, Small-Signal Model for Practical Helix Traveling Wave Tubes Considering the Effects of Severs, Attenuators, and Velocity Tapers. *Journal of the IETE*, Vol. 39, No. 6, 1993.